Density matrix renormalization group simulations of SU(N) Heisenberg chains using standard Young tableaus: Fundamental representation and comparison with a finite-size Bethe ansatz

Pierre Nataf[1,2] and Frédéric Mila[1]

[1]*Institute of Physics, École Polytechnique Fédérale de Lausanne (EPFL), CH-1015 Lausanne, Switzerland*

[2]*Univiversité Grenoble Alpes, CEA INAC-PHELIQS, F-38000, Grenoble, France*

(Received 15 February 2018; published 20 April 2018)

We develop an efficient method to perform density matrix renormalization group simulations of the SU(N) Heisenberg chain with open boundary conditions taking full advantage of the SU(N) symmetry of the problem. This method is an extension of the method previously developed for exact diagonalizations and relies on a systematic use of the basis of standard Young tableaux. Concentrating on the model with the fundamental representation at each site (i.e., one particle per site in the fermionic formulation), we have benchmarked our results for the ground-state energy up to $N = 8$ and up to 420 sites by comparing them with Bethe ansatz results on open chains, for which we have derived and solved the Bethe ansatz equations. The agreement for the ground-state energy is excellent for SU(3) (12 digits). It decreases with N, but it is still satisfactory for $N = 8$ (six digits). Central charges c are also extracted from the entanglement entropy using the Calabrese-Cardy formula and agree with the theoretical values expected from the SU$(N)_1$ Wess-Zumino-Witten conformal field theories.

DOI: 10.1103/PhysRevB.97.134420

I. INTRODUCTION

Continuous progress in ultracold atoms has allowed experimentalists to engineer more and more advanced models of strongly correlated systems. In particular, degenerate gases of strontium and ytterbium loaded in optical lattices have been used to simulate the SU(N) Fermi-Hubbard models [1–8], with N as large as 10. Very recently, the experimental realization of the SU(N) Mott insulating phase was reported [9]. This class of lattice models is a unique playground for strongly correlated systems, as it encompasses a wide variety of quantum ground states with different physical properties. These properties usually depend on the geometry of the lattice (one-dimensional chain, two-dimensional bipartite or frustrated lattice), the number of *colors* (i.e., the value of N), and the local SU(N) symmetry of the wave function [the irreducible representation of SU(N), or more conveniently, the SU(N) *irrep*].

From a theoretical point of view, the study of these lattice models is very challenging. Apart from a few SU(N) models which admit a Bethe ansatz solution [e.g., the SU(N) Heisenberg chain with the fundamental irrep at each site], there is no reliable analytical approach to investigate these models. One then needs to use numerical methods, but they are often of limited efficiency, especially when N is larger than 2 ($N = 2$ corresponds to the familiar Heisenberg spin models). The main reason is the dramatic exponential increase of the dimension of the Hilbert space, which scales as h^{N_s}, where N_s is the number of sites and h is the dimension of the local Hilbert space. In the case of one particle per site, in the fundamental irrep $h = N$, and it is clear that the numerical simulations will become more and more difficult as N increases. In that respect, quantum Monte Carlo simulations are the exception, since a large local Hilbert space is not a major obstacle, but minus-sign-free simulations are only possible in very specific cases [10–14].

One strategy to overcome such a difficulty, and to effectively reduce the relevant number of degrees of freedom in those models, is to *implement* the full SU(N) symmetry in the simulations. Let us take a practical example: In the case of the antiferromagnetic Heisenberg SU(10) model on a 20-site lattice with one particle per site, the implementation of the SU(10) symmetry in an exact diagonalization (ED) algorithm allows one to work directly in the 16 796-dimensional singlet subspace to get the ground state. This dimension is several orders of magnitude smaller than the dimension of the full Hilbert space (around 10^{20}). This is, of course, a huge gain, since the problem has been reduced to the diagonalization of a matrix of dimension $16\,796 \times 16\,796$. However, writing the matrix representing the Hamiltonian in the singlet subspace is in general a difficult task since it makes use of the Clebsch-Gordan coefficients (CGCs), which can only be calculated with an algorithm whose complexity also increases with N [15].

An alternative approach has been developed for exact diagonalizations. It is based on the *orthogonal representation of the symmetric group* [16–18]. A basis for such a representation is provided by the set of standard Young tableaux (SYT), and Alfred Young found out in the 1930s [19,20] very simple rules (the *Young's rules*) to build the matrices representing the elements of the symmetric group in such a basis. The usefulness of the algebraic tools developed to study the representation of the *symmetric* group in the investigation of the Heisenberg SU(N) models is a direct consequence of the *Schur-Weyl duality* [21], which establishes many relations between the representations of the SU(N) groups and the representations of the symmetric groups. A familiar manifestation of the connections between the SU(N) symmetry group and the permutations appears explicitly when one rewrites the Heisenberg interaction $\vec{S}_1 \cdot \vec{S}_2$ between two spins 1/2 as a function of the permutation $P_{1,2}$ as $\vec{S}_1 \cdot \vec{S}_2 = (1/2)P_{1,2} - 1/4$. Thus, it is somehow natural to use the theory of the representation of the symmetric group

to investigate SU(N) models. In particular, the SYTs and the Young's rules allows one to write the matrix representing the SU(N) Heisenberg models in an SU(N) invariant sector [corresponding to an SU(N) irrep] in a very simple manner. It is not obvious, however, to which extent Young's rules and SYTs can also be used to implement the SU(N) symmetry in other numerical methods, such as the density matrix renormalization group (DMRG) [22]. The purpose of this paper is to proceed with such a development.

Note that implementing non-Abelian symmetries [in particular, the SU(N) symmetry] in a DMRG algorithm has already been achieved. For the SU(2) case, several attempts have been successful [23–28]. In most cases, they rely in some way on CGCs. Interestingly, some approaches naturally lead to a formulation where the *colors* are factorized out: for instance, thanks to the Wigner-Eckart theorem, one approach naturally leads to the use of a *reduced basis* [27], or of a *reduced multiplet space* [29]. Through a mapping which transforms a vertex Hamiltonian into an interaction-round-a-face (IRF) Hamiltonian, the DMRG approach from Nishino and Sierra [28] employs as a relevant *reduced basis* the set of *Bratteli diagrams*. In the case of SU(N), these latter are indeed nothing but a graphical way to represent the SYTs. If the set of SYTs is indeed completely equivalent to the different representations of the *reduced basis* used in these approaches, the Young's rules and the orthogonal representation of the symmetric group have unfortunately not been taken full advantage of, while it dramatically reduces the complexity of the calculation of some group theory coefficients which are otherwise based on CGCs. In particular, it allows one to completely shortcut the difficult calculation of the $3n-j$ symbols, which are useful to calculate the reduced matrix elements appearing in the Wigner-Eckart theorem and are necessary to calculate the matrix elements between the states of the *reduced basis*. Improving the computation of such coefficients is indeed not just an optimization problem. As pointed out by Weichselbaum, whose general framework does not apply only to SU(N) invariant groups but to other non-Abelian groups as well [29], developing a strategy to shortcut the sum rules and contraction of complex networks of CGC space is of crucial importance to implement symmetries with rank (i.e., the value of N) higher than 3. The use of Young's rules and SYTs is a way to implement this strategy, and it has enabled us to study the SU(8) Heisenberg chain almost as easily as the SU(4) Heisenberg chain. In the following, we develop this method.

In Sec. II A, we describe our procedure, which is based on the original formulation of DMRG by White. Such a framework was the most natural one to use the Young's rules in a relatively simple manner. We apply our formalism to the Heisenberg SU(N) chain, with one particle per site in the fundamental irrep and with open boundary conditions (OBC), but many of the concepts developed here can be generalized to other models. We put more emphasis on the parts where Young's rules have proven to be particularly convenient to make the group theory calculations needed for the computation. Then, in order to have proper numerical values to benchmark our code, we explicitly write and solve the Bethe ansatz equations for the SU(N) chain with OBC in Sec. III. In Sec. II, we compare the results from our DMRG code to the exact results for SU(3) up to SU(8), calculate the central charges for a chain of several hundreds of sites, and demonstrate some good agreement with the expected $\mathrm{SU}(N)_1$ conformal field theory (CFT) behavior. Then, conclusions and perspectives are drawn. Finally, some results about the orthogonal representation of the symmetric group are reported in the Appendix. Among other things, it is shown that this representation makes the determination of the IRF weights needed in the DMRG formulation of Nishino and Sierra [28] for SU(2) essentially trivial.

II. DMRG WITH IMPLEMENTATION OF THE FULL SU(N) SYMMETRY

A. Structure of the DMRG code

We present below a description of the DMRG algorithm with implementation of the full SU(N) symmetry for the case of the antiferromagnetic Heisenberg SU(N) chain with one particle per site, i.e., with the fundamental irrep at each site. Most of the ideas described below can be generalized to Hamiltonians with other irreps of SU(N) and/or other one-dimensional geometries such as ladders. We will concentrate on the stages where the use of SYT proves to be both convenient and powerful for the calculation of some group theory coefficients which are necessary for the implementation of the SU(N) symmetry. The calculation of these coefficients becomes intractable without SYTs when N increases (larger than 4 typically). The infinite-size DMRG algorithm we present below is based on White's original idea: the L-site chain is split into two half-chains of size $L/2$ (the *left* block and the *right* block, as shown in Fig. 1), and one lets them grow by adding one site at a time. To prevent the dimension of the Hilbert space on both blocks from becoming too large, one then applies the density matrix truncation in order to keep a number of states on both blocks not higher than m, which is one of the input parameters of the algorithm. Once the desired length of the chain is reached, the infinite-size part of the DMRG is finished and one starts the finite-size part, which consists in performing some sweeps, allowing one to gain some accuracy on the ground-state energy and to determine, for instance, the profile of the entanglement entropy. We will focus below on the infinite-size part of the DMRG, since most of the issues raised by the implementation of the SU(N) symmetry in this part appear in a very similar way in the finite-size part. Before describing one step of the infinite DMRG, let us explain the truncation scheme we have chosen. In addition to the usual density matrix truncation, which involves the selection for the left (or the right) block of the m states of largest eigenvalues in

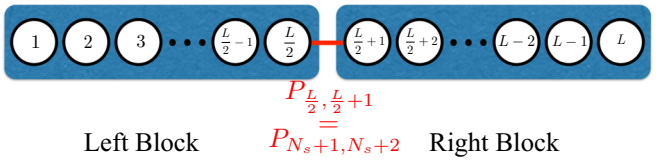

FIG. 1. Sketch of the indexing of the L-site chain (L even) split into two parts: the left block and the right block. Each block has length $L/2 = N_s + 1$. The interaction between the two blocks is the permutation between the last site of the left block and the first site of the right block, i.e., $P_{\frac{L}{2},\frac{L}{2}+1} = P_{N_s+1,N_s+2}$.

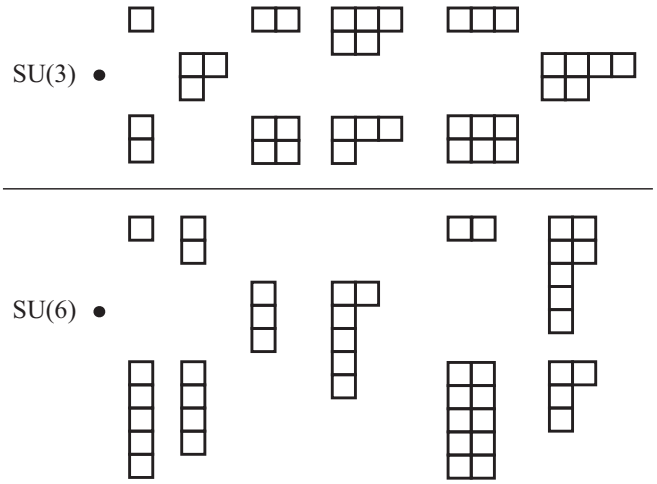

FIG. 2. First eleven irreps of SU(3) (top) and SU(6) (bottom), ordered from left to right according to the ascending quadratic Casimir. Pairs of conjugate irreps are put one above the other since they have the same quadratic Casimir. The singlet irrep is drawn with a dot. The truncation scheme is such that we consider only the states belonging to the first M irreps, where M is an input parameter of the DMRG algorithm (see text for details).

the diagonalization of the reduced density matrix, we perform a truncation on the SU(N) irreps as well.

Only the states living in the M irreps of lowest quadratic Casimir will be taken into account, where M is an input parameter of the algorithm. This is well adapted to antiferromagnetic problems since the low energy states live in those irreps, and it allows one to calculate a **finite** number of group theory coefficients (see Sec. II C) needed for the computation *once for all* before the simulation starts. Typically, for M around 100 or 200, the accuracy is already very good for $m = 1000$, as we will see in Sec. II. Such a list for SU(3) and for SU(6) with $M = 11$ is shown in Fig. 2. The quadratic Casimir C_2 depends on the shape of an SU(N) irrep $\alpha = [\alpha_1,\alpha_2,\ldots,\alpha_k]$, with α_i the length of row i of the shape and k the number of rows of the shape as [30]

$$C_2 = \frac{1}{2}\left\{ n\left(N - \frac{n}{N}\right) + \sum_{i=1}^{k} \alpha_i^2 - \sum_{j=1}^{j=\alpha_1} c_j^2 \right\}, \qquad (1)$$

where the c_j ($j = 1,..,\alpha_1$) are the lengths of the columns, and n is the number of boxes of the irrep.

B. Description of one step of the infinite DMRG

We explain here how to pass from the stage where both the *left* and the *right* blocks have N_s sites to the stage where they both have $N_s + 1$ sites. We focus on the left block (which is perfectly mirror symmetric to the right block in the infinite-size DMRG), and we assume that we have kept in memory $m_{N_s} \leqslant m$ states from the previous stage, each of them belonging to a given SU(N) symmetry sector labeled by one Young tableau (YT) or *shape* α with N_s boxes. Before going further, let us make a remark: There are different conventions to represent the same SU(N) irrep α, with or without the columns of N boxes; for instance, for SU(3), we have

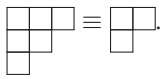

(2)

1. Selection of states for the current step

Each Young tableau of N_s boxes to be considered should be present in the list of M YTs. In Fig. 3, where $N_s = 5$, the selected YTs for stage N_s are shown in green. The first two are allowed, although they have only two boxes because one can add a column with three boxes to reach $N_s = 5$ boxes. There are $M_{N_s} \leqslant M$ such shapes. For each sector α, we have kept $m^{\alpha}_{N_s}$ states that we can write as

$$\left\{ \left|\zeta_1^{\alpha}\right\rangle, \left|\zeta_2^{\alpha}\right\rangle, \ldots, \left|\zeta_{m^{\alpha}_{N_s}}^{\alpha}\right\rangle \right\}. \qquad (3)$$

The number of states $m^{\alpha}_{N_s}$ satisfies

$$\sum_{\alpha} m^{\alpha}_{N_s} = m_{N_s}, \qquad (4)$$

where the sum runs over the M_{N_s} shapes α with N_s boxes present in the list of M irreps.

The states in Eq. (3) are the eigenstates of the $m^{\alpha}_{N_s} \times m^{\alpha}_{N_s}$ reduced density matrix ρ^{α}. (We will show later how to calculate the reduced density matrix for a given sector α.) The corresponding positive eigenvalues are ranked from the largest to the lowest: $\{\lambda_1^{\alpha},\lambda_2^{\alpha},\ldots,\lambda^{\alpha}_{m^{\alpha}_{N_s}}\}$. In addition, we also assume that from the previous stage we have kept the matrices $\mathcal{H}^{\alpha}_{N_s}$, which are the matrices of the Heisenberg Hamiltonian H_{N_s} with OBC for N_s sites, expressed in the basis of Eq. (3): the (i,j) coefficient of $\mathcal{H}^{\alpha}_{N_s}$ is $(\mathcal{H}^{\alpha}_{N_s})_{i,j} = \langle\zeta_i^{\alpha}|H_{N_s}|\zeta_j^{\alpha}\rangle$.

To add one site to the left block, we first need to identify the $M_{N_s+1} \leqslant M$ shapes β containing $N_s + 1$ boxes and belonging to the list of M irreps. (They are shown in red in Fig. 3 where $N_s = 5$.)

Then we need to select m_{N_s+1} states which will live in the ensemble of M_{N_s+1} sectors β. To perform such a selection of states (which is indeed nothing but the density matrix truncation), we proceed as follows: For each shape β, we consider all the possible *ascendant* shapes α made of N_s boxes. They are such that β belongs to the tensor product $\alpha \otimes \square$, where $\square$ is the fundamental irrep. We denote the number of ascendant shapes by $n_{asc}(\beta)$. Each ascendant of β, which we denote by α_k^{β} [for $k = 1,\ldots,n_{asc}(\beta)$] is obtained by deleting one *bottom corner* from β. (See Fig. 4 for a definition and some examples of bottom corners.)

Then, for each β, we create the list L_{β} of eigenvalues of ρ^{α} for α an ascendant shape, i.e., $\alpha \in \{\alpha_1^{\beta},\alpha_2^{\beta},..,\alpha^{\beta}_{n_{asc}(\beta)}\}$:

$$L_{\beta} = \left\{\lambda_q^{\alpha}\right\}_{q=1,\ldots,m^{\alpha}_{N_s}}^{\alpha\in\{\alpha_1^{\beta},\alpha_2^{\beta},\ldots,\alpha^{\beta}_{n_{asc}(\beta)}\}}. \qquad (5)$$

One then creates L_{N_s+1}, the union of these lists over the M_{N_s+1} shapes β: $L_{N_s+1} = \bigcup_{\beta} L_{\beta}$. Note that if a N_s box shape α gives rise to several different *descendant* shapes when adding the fundamental irrep, its associated values λ_q^{α} (for $q = 1,\ldots,m^{\alpha}_{N_s}$) will appear several times in L_{N_s+1}. Then we choose the m_{Ns+1} largest values in L_{N_s+1}, where $m_{Ns+1} = \mathrm{Min}[m,\mathrm{cardinal}(L_{N_s+1})]$. The labels attached to each of the chosen $\lambda_q^{\alpha_k^{\beta}}$ allow one to select for each sector β, $m^{\beta}_{N_s+1}$

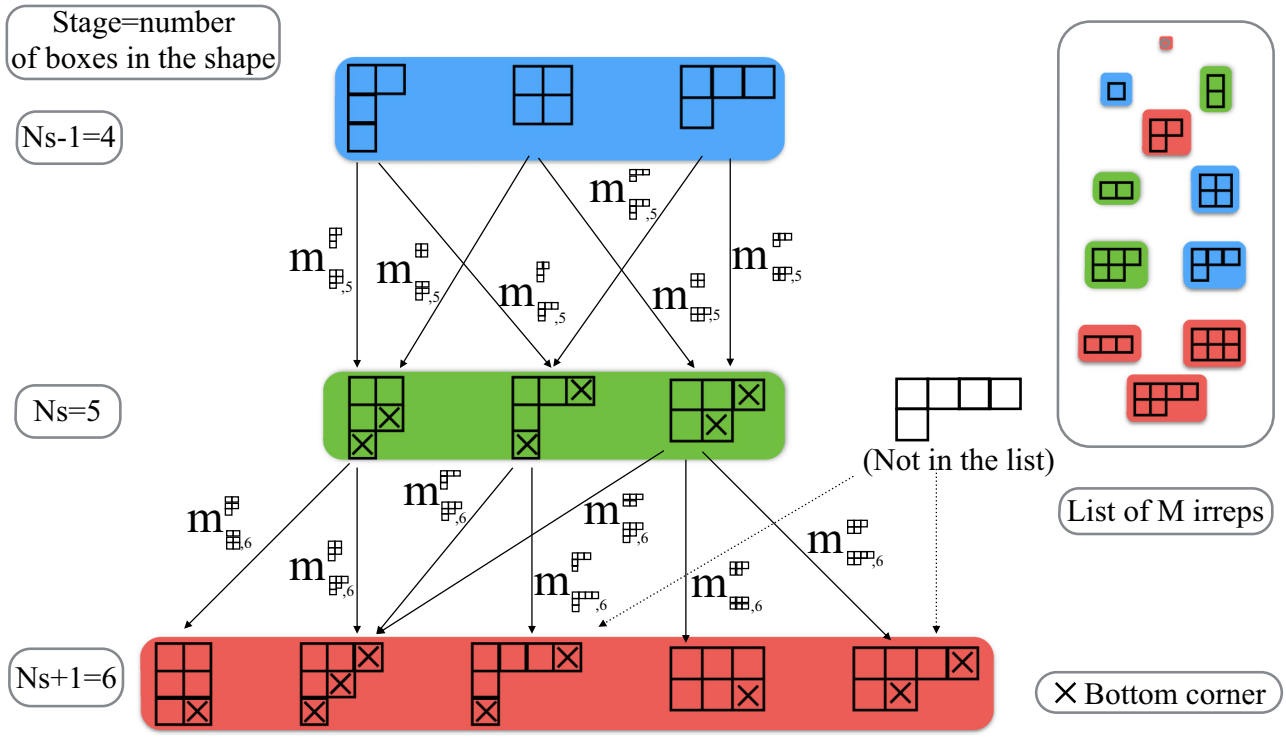

FIG. 3. Scheme of the selection of states for SU(3) and $N_s = 5$. Each state belongs to a sector labeled by a Young tableau, or shape, which is present in the list of M irreps. Such a list is shown on the right for $M = 11$. Each shape β at stage $N_s + 1$ has $n_{acs}(\beta)$ ascendant shapes $\alpha \in \{\alpha_1^\beta, \alpha_2^\beta, ..., \alpha_{n_{asc}(\beta)}^\beta\}$ coming from the stage N_s, which can be obtained from β by deleting one bottom corner (see also Fig. 4 for a definition). The sector associated to β is spanned by a set of states built from the states coming from the previous stage, and living in the sectors labeled by α_k^β for $k = 1...n_{acs}(\beta)$. The *genealogy* of each state (up to the *grandparent* level) and the *Young rules* (see Sec. A 2 for a review) are the unique ingredients needed to build the whole algorithm (see text for details).

ascendant states. We call σ_β the sum of the corresponding eigenvalues. Each selected state comes from one of the $n_{asc}(\beta)$ ascendant shapes α_k^β. We finally denote by m^α_{β,N_s+1} the number of selected states belonging to the sector β (shapes with $N_s + 1$ boxes) coming from the ascendant sector α (shapes with N_s boxes), so that $m^\beta_{N_s+1} = \sum_\alpha m^\alpha_{\beta,N_s+1}$. In Fig. 3, we give a practical example to illustrate the selection we have described in this section. Let us note that other selection schemes exist.

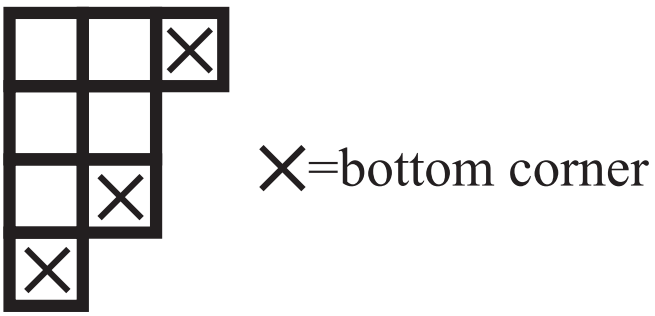

FIG. 4. For a given *Young tableau* $\beta = [\beta_1, \beta_2, \ldots, \beta_k]$, with β_i the length of row i of the shape and k the number of rows of the shape (here $\beta = [3221]$ and $k = 4$), the bottom corners are the boxes where we could put the last number when we fill up the shape in the *standard way*. (Here, the last number, which is also the total number of boxes, is equal to 8.) If we conventionally set $\beta_{k+1} = 0$, those bottom corners correspond to all the rows j such that $\beta_j > \beta_{j+1}$.

For instance, the set of numbers $\{m^\beta_{N_s+1}\}_\beta$ can be imposed as an input parameter (as in [31]), but for a given number of states $\sum_\beta m^\beta_{N_s+1}$, this scheme is less efficient than the protocol shown here, which automatically selects the best set $\{m^\beta_{N_s+1}\}_\beta$.

Finally, the *weight* which is discarded as a consequence of the truncation is given by

$$\mathcal{W}_d^L = 1 - \sum_\beta g_\beta \sigma_\beta. \tag{6}$$

In this expression, the factor $g_\beta = \dim(\beta)/h$, where $\dim(\beta)$ is the dimension of the SU(N) irrep of shape β (see Sec. A 1 for a way to calculate such a dimension directly from the shape β), and where h is the dimension of the local Hilbert space. In the present case, $h = \dim(\square) = N$. The factor g_β comes from the normalization condition of the reduced density matrices (see also Sec. II B 4) and from the enhancement of the dimension of the full Hilbert space when one site is added to the left block.

2. Construction of the new matrices for the left block

In this section, we explain how to build $\mathcal{H}^\beta_{N_s+1}$, the matrix representing the antiferromagnetic Heisenberg Hamiltonian H_{N_s+1} with OBC for $N_s + 1$ sites in each sector β (shapes with $N_s + 1$ boxes). First of all, one can write H_{N_s+1} as

$$H_{N_s+1} = H_{N_s} + P_{N_s,N_s+1}, \tag{7}$$

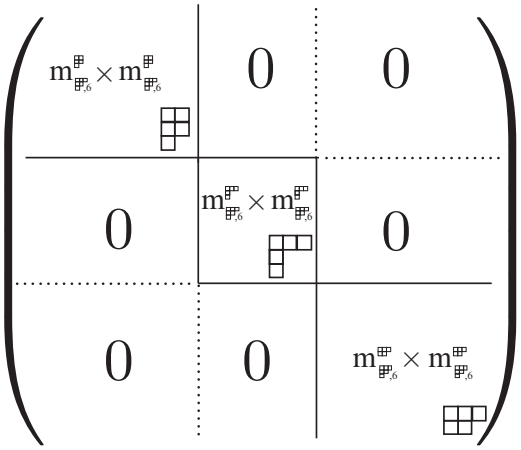

FIG. 5. Matrix $\mathcal{H}^{\beta}_{N_s}$, which represents H_{N_s} (here $N_s = 5$), in the sector $\beta =$  . It is block diagonal; each block is associated to a shape α which is an ascendant of β (and which is called α^{β}_k for $k = 1, \ldots, n_{asc}(\beta)$ in the text) and has dimension $m^{\alpha}_{\beta,N_s+1} \times m^{\alpha}_{\beta,N_s+1}$. The matrix representing H_{N_s+1} in sector β will be the sum of $\mathcal{H}^{\beta}_{N_s}$ and of another matrix $\mathcal{P}^{\beta}_{N_s,N_s+1}$ (see text for details).

where H_{N_s} is the Heisenberg Hamiltonian for N_s sites with OBC, and where P_{N_s,N_s+1} is the interaction term between site N_s and site $N_s + 1$. The $m^{\beta}_{N_s+1} \times m^{\beta}_{N_s+1}$ matrix $\mathcal{H}^{\beta}_{N_s+1}$ will be written as the sum of the matrix representing H_{N_s} and P_{N_s,N_s+1}, respectively, in sector β. We know from the previous part that sector β can be split into $n_{asc}(\beta)$ subsectors, each of them corresponding to an ascendant shape α^{β}_k $[k = 1, \ldots, n_{asc}(\beta)]$, of dimension $m^{\alpha^{\beta}_k}_{\beta,N_s+1}$.

First, since we have kept in memory from the previous stages the matrices $\mathcal{H}^{\alpha}_{N_s}$, the construction of the matrix representing H_{N_s} in sector β requires just the concatenation of the submatrices $(\mathcal{H}^{\alpha}_{N_s})_{i,j}$, where $1 \leqslant i \leqslant m^{\alpha}_{\beta,N_s+1}, 1 \leqslant j \leqslant m^{\alpha}_{\beta,N_s+1}$, for $\alpha = \alpha^{\beta}_k$ $[k = 1, \ldots, n_{asc}(\beta)]$. The matrix $\mathcal{H}^{\beta}_{N_s}$, which represents H_{N_s} in sector β, will then be block diagonal, each block corresponding to a subsector α^{β}_k $[k = 1, \ldots, n_{asc}(\beta)]$, as illustrated in Fig. 5.

Now, the construction of the matrix $\mathcal{P}^{\beta}_{N_s,N_s+1}$, which represents P_{N_s,N_s+1} in the sector β, requires two kinds of ingredients:

(1) The set of numbers $\{m^{\alpha}_{\beta,N_s+1}\}_{\alpha \in \{\alpha^{\beta}_1, \alpha^{\beta}_2, \ldots, \alpha^{\beta}_{n_{asc}(\beta)}\}}$ and $\{m^{\chi}_{\alpha,N_s}\}_{\chi \in \{\chi^{\alpha}_1, \chi^{\alpha}_2, \ldots, \chi^{\alpha}_{n_{asc}(\alpha)}\}}$ for $\alpha = \alpha^{\beta}_k$ $[k = 1, \ldots, n_{asc}(\beta)]$. The shapes $\chi \in \{\chi^{\alpha}_1, \chi^{\alpha}_2, \ldots, \chi^{\alpha}_{n_{asc}(\alpha)}\}$ are the shapes with $N_s - 1$ boxes which are ascendant of a given shape α.

(2) The set of wave functions $\{|\zeta^{\alpha}_1\rangle, |\zeta^{\alpha}_2\rangle, \ldots, |\zeta^{\alpha}_{m^{\alpha}_{N_s}}\rangle\}, \forall \alpha = \alpha^{\beta}_k$ $[k = 1, \ldots, n_{asc}(\beta)]$.

The sectors α being split into different subsectors χ, the coefficients of the corresponding wave functions $|\zeta^{\alpha}_q\rangle$ (for $q \leqslant m^{\alpha}_{\beta,N_s+1}$) are decomposed accordingly. Then, for the coefficient $\langle \zeta^{\alpha}_i | P_{N_s,N_s+1} | \zeta^{\alpha'}_j \rangle$ (with $\alpha, \alpha' \in \{\alpha^{\beta}_1, \alpha^{\beta}_2, .., \alpha^{\beta}_{n_{asc}(\beta)}\}$ and $1 \leqslant i \leqslant m^{\alpha}_{\beta,N_s+1}$ and $1 \leqslant j \leqslant m^{\alpha'}_{\beta,N_s+1}$) to be nonzero, α and α' must have one common ascendant shape χ. From the shapes χ, β, α, and α', the calculation of $\langle \zeta^{\alpha}_i | P_{N_s,N_s+1} | \zeta^{\alpha'}_j \rangle$ becomes trivial thanks to the rules defining the orthogonal representation of the symmetric group (Young's rules) that are reviewed in the Appendix (in Sec. A 2). This set of rules describes the action of the permutation Hamiltonian term over the basis of SYTs. In particular, the action of P_{N_s,N_s+1} just depends on the location of the bottom corner from stage $N_s - 1$ to stage N_s, and on the location of the bottom corner from stage N_s to $N_s + 1$. This information is contained in the chains $\chi \to \alpha \to \beta$ (and $\chi \to \alpha' \to \beta$), as illustrated in Fig. 6.

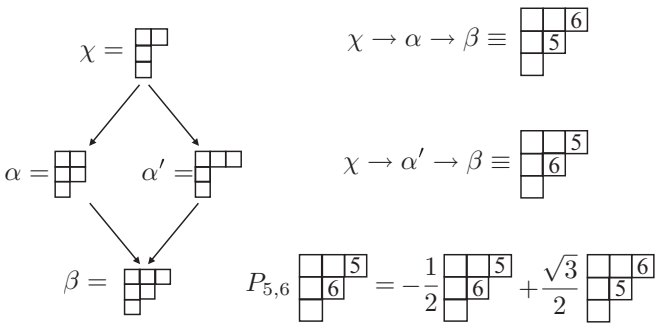

FIG. 6. To create the matrix $\mathcal{P}^{\beta}_{N_s,N_s+1}$, which represents P_{N_s,N_s+1} in the sector β (here $\beta =$  and $N_s = 5$), one just needs to keep track of the *chains* $\chi \to \alpha \to \beta$ and $\chi \to \alpha' \to \beta$, where α and α' are two ascendant shapes of β and χ is a common ascendant shape of both α and α'. Then one uses the rules of the orthogonal representation of the symmetric group (Young's rules) reviewed in the Appendix (Sec. A 2) to know the effect of P_{N_s,N_s+1} on the states living in sector β and subsectors α and α'.

Interestingly, in the IRF-DMRG approach that can be used for the SU(2) Heisenberg chain, the matrix elements $\langle \zeta^{\alpha}_i | P_{N_s,N_s+1} | \zeta^{\alpha'}_j \rangle$ are expressed in terms of the "Boltzmann (or IRF) weights." The calculation of these coefficients becomes trivial using Young's rules, as we show in the Appendix, Sec. A 3.

3. Building the matrix for the superblock

So far, we have been able to create the matrices representing the antiferromagnetic Heisenberg Hamiltonian H_{N_s+1} with OBC for $N_s + 1$ sites in every sector β (shapes with $N_s + 1$ boxes), where β is one of the M_{N_s+1} shapes present in the list of the M SU(N) irreps. From now on, we index those shapes by $\beta \equiv \beta_q$ $(q = 1, \ldots, M_{N_s+1})$, which are ordered according to their quadratic Casimir. We are going to use the matrices $\mathcal{H}^{\beta_q}_{N_s+1}$ $(q = 1, \ldots, M_{N_s+1})$ for our next goal: finding the ground state $|GS\rangle_L$ of the antiferromagnetic Heisenberg Hamiltonian H_L with OBC for $L = 2N_s + 2$ sites, which corresponds to the *union* of the left and the right block, as shown in Fig. 1. To achieve this purpose, one can first build the matrix representing H_L on the SU(N) sector where $|GS\rangle_L$ lives. Such a sector is labeled by a shape made of L boxes and is clearly model dependent. In our case (antiferromagnet with the fundamental irrep at each site), such a shape is equivalent to the column with $rem(L,N)$ boxes, where $rem(L,N)$ is the rest in the Euclidean division of L by N. For instance, if $L = 12$ and $N = 3$, $|GS\rangle_L$ will be an SU(3) singlet. Once such a sector γ_L is identified, we

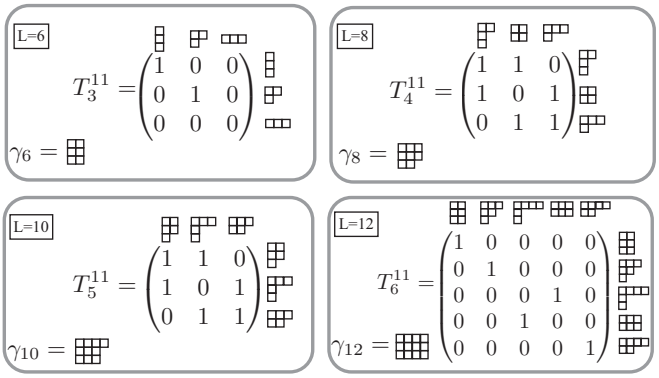

FIG. 7. Examples of shapes γ_L and matrices $T^{M=11}_{N_s+1}$ for different sizes, from $L=6$ (top left) to $L=12$ (bottom right), for SU(3). The shape γ_L is the SU(3) irrep containing the ground state for the antiferromagnetic Heisenberg SU(3) spin chain with L sites with OBC and the fundamental irrep at each site. The shapes β_q ($q=1,\ldots,M_{N_S+1}$) which label the columns (resp. lines) of the matrices $T^{M=11}_{N_s+1}$ represent the SU(N) irreps for the left (resp. right) block made of $N_s+1=L/2$ sites. The entries $T^{11}_{N_s+1}(q,q')=1$ if $\gamma_L \in \beta_q \otimes \beta_{q'}$ and 0 otherwise (see text for details). For instance, $T^{11}_5(2,1)=1$ because 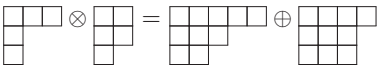 contains γ_{10}.

need to create the Hilbert space of the associated *superblock* and to write the matrix representing H_L in it. To reach this goal, one first calculates the $M_{N_s+1}\times M_{N_s+1}$ Boolean (and symmetric) matrix $T^M_{N_s+1}$ defined for $1\leqslant q,q'\leqslant M_{N_s+1}$ as

$$\begin{aligned} T^M_{N_s+1}(q,q')&=1 \Leftrightarrow \gamma_L \in \beta_q\otimes\beta_{q'}\\ T^M_{N_s+1}(q,q')&=0 \ \text{ otherwise,}\end{aligned} \tag{8}$$

where $\gamma_L \in \beta_q\otimes\beta_{q'}$ means that γ_L appears in the tensor product of the SU(N) irreps β_q and $\beta_{q'}$. To perform such a tensor product, one can, for instance, use the Itzykson-Nauenberg rules [32]. In Fig. 7, we give the matrices $T^M_{N_s+1}$ for SU(3), $M=11$ (see the list shown in Fig. 2), for $N_s+1=3$ up to $N_s+1=6$.

We then list the $M^{GS}_{N_S+1}\leqslant M_{N_S+1}$ *relevant* shapes β_k (for $1\leqslant k\leqslant M_{N_S+1}$), which are such that the column $T^M_{N_s+1}(:,k)$ has at least one nonzero entry. We write them $\tilde\beta_k$ (for $k=1,\ldots,M^{GS}_{N_S+1}$). For instance, for SU(3), $L=6$ and $M\geqslant 9$, there are $M_3=3$ shapes β_q:

$$\begin{aligned}\beta_1 &= \\ \beta_2 &= \\ \beta_3 &= \end{aligned} \tag{9}$$

But as shown in Fig. 7, since the third column of T^{11}_3 has only vanishing entries, contrary to the first two columns, $M^{GS}_3=2$ and the two relevant shapes are $\tilde\beta_1=$  and $\tilde\beta_2=$ 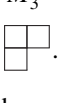 . The shape 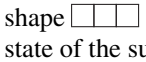 does not participate in the creation of the ground state of the superblock.

The Hilbert space of the superblock on sector γ_L is then the tensor product of the direct sum of the sectors corresponding to the shapes $\tilde\beta_k$ (for $k=1,\ldots,M^{GS}_{N_S+1}$) for the left block with the same direct sum for the right block. Consequently, its dimension is $\tilde m^2_{N_s+1}$, where $\tilde m_{N_s+1}=\sum_{k=1}^{M^{GS}_{N_S+1}} m^{\tilde\beta_k}_{N_s+1}$. In practice, after a few starting steps, we observe that $\tilde m_{N_s+1}=m_{N_s+1}=m$. The ground-state wave function will thus be written as

$$|GS\rangle_L=\sum_{i,i',k,k'}\Psi^{|GS\rangle_L}_{i,i',k,k'}|\eta^{\tilde\beta_k}_i\rangle\otimes|\eta^{\tilde\beta_{k'}}_{i'}\rangle, \tag{10}$$

where the sum runs over the indices i,i',k,k', which are such that $1\leqslant k,k'\leqslant M^{GS}_{N_S+1}$, $1\leqslant i\leqslant m^{\tilde\beta_k}_{N_s+1}$, and $1\leqslant i'\leqslant m^{\tilde\beta_{k'}}_{N_s+1}$, and where the states $|\eta^{\tilde\beta_k}_i\rangle$ are the states of sector $\tilde\beta_k$. (See the previous section for the way we built the corresponding sector.) Now that we know the Hilbert space for the superblock, let us write $\mathcal{H}^{\gamma_L}_L$, the matrix representing H_L in this space. First, we can decompose H_L as

$$H_L=H^{\text{Left}}_{N_s+1}+H^{\text{Right}}_{N_s+1}+P_{N_s+1,N_s+2}, \tag{11}$$

where $H^{\text{Left}}_{N_s+1}$ is the Heisenberg Hamiltonian with OBC for the left block (for site 1 up to site N_s+1), $H^{\text{Right}}_{N_s+1}$ is the Heisenberg Hamiltonian with OBC for the right block (for site N_s+2 up to site $2N_s+2$), and P_{N_s+1,N_s+2} is the interaction term between the last site of the left block (indexed by N_s+1) and the first site of the right block (indexed by N_s+2). We illustrate this indexing in Fig. 1. The calculation of the matrix $\mathcal{P}^{\gamma_L}_{N_s+1,N_s+2}$, which represents P_{N_s+1,N_s+2} (on the sector γ_L), is made easy thanks to the SYTs through the use of the *subduction* coefficients. We will focus on this task in a devoted paragraph (see Sec. II C).

The matrices $\mathcal{H}^{\text{Left}}_{N_s+1}$ and $\mathcal{H}^{\text{Right}}_{N_s+1}$, respectively representing $H^{\text{Left}}_{N_s+1}$ and $H^{\text{Right}}_{N_s+1}$ on sector γ_L of the superblock, are simply

$$\begin{aligned}\mathcal{H}^{\text{Left}}_{N_s+1}&=\bigoplus_{T^M_{N_s+1}(q,q')=1}\mathcal{H}^{\beta_q}_{N_s+1}\otimes\mathcal{I}^{\beta_{q'}}_{N_s+1}\\ \mathcal{H}^{\text{Right}}_{N_s+1}&=\bigoplus_{T^M_{N_s+1}(q',q)=1}\mathcal{I}^{\beta_{q'}}_{N_s+1}\otimes\mathcal{H}^{\beta_q}_{N_s+1},\end{aligned} \tag{12}$$

where $\mathcal{I}^{\beta}_{N_s+1}$ is the $m^{\beta}_{N_s+1}\times m^{\beta}_{N_s+1}$ identity matrix on the sector labeled by shape β (for $\beta\in\{\tilde\beta_1,\tilde\beta_2,\ldots,\tilde\beta_{M^{GS}_{N_S+1}}\}$).

4. Preparing the next stage

To finish this stage of the algorithm, one first calculates the ground state $|GS\rangle_L$, which is the eigenvector of minimal energy (that we will call $\mathcal{E}_L$) of $\mathcal{H}^{\gamma_L}_L$, using, for instance, the Lanczos algorithm. Then we need to calculate the reduced density matrices $\rho^{\tilde\beta_k}$ (for $k=1,\ldots,M^{GS}$), whose coefficients are defined (for $1\leqslant i,j\leqslant m^{\tilde\beta_k}_{N_s+1}$) as

$$\rho^{\tilde\beta_k}(i,j)=\frac{1}{\dim(\tilde\beta_k)}\sum_{i',k'}\left(\Psi^{|GS\rangle_L}_{i,i',k,k'}\right)^*\Psi^{|GS\rangle_L}_{j,i',k,k'}, \tag{13}$$

where $\dim(\tilde\beta_k)$ is the dimension of the SU(N) irrep of shape $\tilde\beta_k$. The factor $1/\dim(\tilde\beta_k)$ guarantees the correct normalization of the reduced density matrices. This is completely analogous

to Eqs. (68)–(69) in Ref. [28], which deals with the SU(2) case. This factor, together with the factor g_β defined below Eq. (6) of the present paper, are also consistent with the factor defined in Eq. (18) of Ref. [29].

We then diagonalize the reduced density matrices to obtain the set of eigenvalues ranked from largest to lowest, $\{\lambda_1^{\tilde\beta_k},\lambda_2^{\tilde\beta_k},\ldots,\lambda_{m_{N_s+1}^{\tilde\beta_k}}^{\tilde\beta_k}\}$, as well as the corresponding eigenvectors:

$$\left\{\left|\zeta_1^{\tilde\beta_k}\right\rangle,\left|\zeta_2^{\tilde\beta_k}\right\rangle,\ldots,\left|\zeta_{m_{N_s+1}^{\tilde\beta_k}}^{\tilde\beta_k}\right\rangle\right\}, \tag{14}$$

and we perform a rotation to reexpress $\mathcal{H}_{N_s+1}^{\tilde\beta_k}$ in the basis shown in Eq. (14), for $k=1,\ldots,M^{GS}$. We keep in memory those quantities for the next stage. At this step, one can also calculate the entanglement entropy $S(L)$ as

$$S(L)=-\sum_{k=1}^{M_{N_S+1}^{GS}}\dim(\tilde\beta_k)\rho^{\tilde\beta_k}\log(\rho^{\tilde\beta_k}). \tag{15}$$

Note that the matrices representing the Heisenberg Hamiltonian in the irrelevant sectors, i.e.,

$$\mathcal{H}_{N_s+1}^{\beta}\ \text{for}\ \beta\notin\left\{\tilde\beta_1,\tilde\beta_2,\ldots,\tilde\beta_{M_{N_S+1}^{GS}}\right\},$$

do not undergo any transformation at this step; furthermore, the values λ^β for such sectors are null.

C. Calculation of the matrix representing the interaction between the left and the right block using the permutational subduction coefficients

In this section, we show how to calculate the matrix $\mathcal{P}_{N_s+1,N_s+2}^{\gamma_L}$, which represents the interblock interaction term P_{N_s+1,N_s+2} on sector γ_L. To simplify the notation, all along this part we will drop the indices in $\mathcal{P}_{N_s+1,N_s+2}^{\gamma_L}$ and simply call it $\mathcal{P}_{\gamma_L}$.

First of all, for $\beta_{q_1},\beta_{q_2},\beta_{q_3},\beta_{q_4}\in\{\tilde\beta_1,\tilde\beta_2,\ldots,\tilde\beta_{M_{N_S+1}^{GS}}\}$ and for i_j such that $1\leqslant i_j\leqslant m_{N_s+1}^{\beta_{q_j}}$ (for $j=1,..,4$), the coefficients $\langle\eta_{i_3}^{\beta_{q_3}}|\otimes\langle\eta_{i_4}^{\beta_{q_4}}|\mathcal{P}_{\gamma_L}|\eta_{i_1}^{\beta_{q_1}}\rangle\otimes|\eta_{i_2}^{\beta_{q_2}}\rangle$ will be zero unless

$$T_{N_s+1}^{M}(q_1,q_2)=T_{N_s+1}^{M}(q_3,q_4)=1\qquad\text{Condition (1)}, \tag{16}$$

which means that both $\gamma_L\in\beta_{q_1}\otimes\beta_{q_2}$ and $\gamma_L\in\beta_{q_3}\otimes\beta_{q_4}$.

Another condition is that the subsectors where the states $|\eta_{i_1}^{\beta_{q_1}}\rangle$ and $|\eta_{i_3}^{\beta_{q_3}}\rangle$ live (see Fig. 5 for a way sectors β are split into different subsectors) should correspond to the same ascendant shape:

$$\alpha=\alpha_{k_1}^{\beta_{q_1}}=\alpha_{k_3}^{\beta_{q_3}}\qquad\text{Condition (2)} \tag{17}$$

for some indices $1\leqslant k_j\leqslant n_{asc}(\beta_{q_j})$ for $j=1,3$. And the same condition applies for the other pair of states $|\eta_{i_2}^{\beta_{q_2}}\rangle$ and $|\eta_{i_4}^{\beta_{q_4}}\rangle$:

$$\alpha'=\alpha_{k_2}^{\beta_{q_2}}=\alpha_{k_4}^{\beta_{q_4}}\qquad\text{Condition (3)} \tag{18}$$

for some indices $1\leqslant k_j\leqslant n_{asc}(\beta_{q_j})$ for $j=2,4$.

The coefficients $\langle\eta_{i_3}^{\beta_{q_3}}|\otimes\langle\eta_{i_4}^{\beta_{q_4}}|\mathcal{P}_{\gamma_L}|\eta_{i_1}^{\beta_{q_1}}\rangle\otimes|\eta_{i_2}^{\beta_{q_2}}\rangle$ then will only depend on the four chains which determine the subsectors included in the sectors β_{q_j} where the states $|\eta_{i_j}^{\beta_{q_j}}\rangle$ live (for $j=1,2,3,4$):

$$\begin{aligned}\alpha&\to\beta_{q_1}\\ \alpha&\to\beta_{q_3}\\ \alpha'&\to\beta_{q_2}\\ \alpha'&\to\beta_{q_4}.\end{aligned} \tag{19}$$

We can keep track of this information using the shapes β_{q_j} and the bottom corners which reveal which ascendant shape each state $|\eta_{i_j}^{\beta_{q_j}}\rangle$ (for $j=1,2,3,4$) comes from. For instance, for $N_s+1=5$ and SU(3), as will be shown in the next subsection,

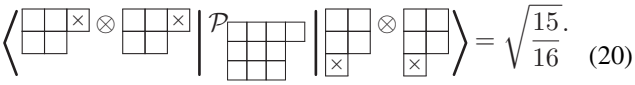

$$=\sqrt{\frac{15}{16}}. \tag{20}$$

Let us as illustrate the implications of conditions (1), (2), and (3) using this notation. Condition (1) implies that

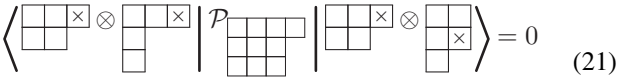

$$=0 \tag{21}$$

since $T_5^{11}(3,1)=0$ as shown in Fig. 7. Condition (2) leads, for instance, to

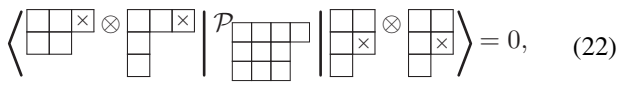

$$=0, \tag{22}$$

while

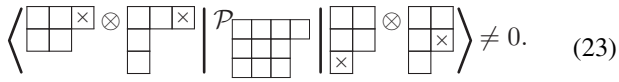

$$\neq 0. \tag{23}$$

And condition (3) implies that

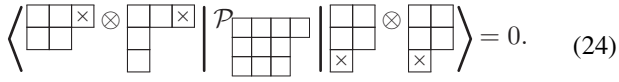

$$=0. \tag{24}$$

Finally, we should keep in mind that we are dealing with SU(N) irreps, so the coefficients for two ensembles of shapes which are equivalent, $\{\beta_{q_1},\beta_{q_2},\beta_{q_3},\beta_{q_4}\}\equiv\{\beta'_{q_1},\beta'_{q_2},\beta'_{q_3},\beta'_{q_4}\}$, should be the same. In particular, the coefficients appearing in $\mathcal{P}_{\gamma_L}$ at stage N_s+pN (p integer) should be the same as the ones appearing at stage N_s. For instance,

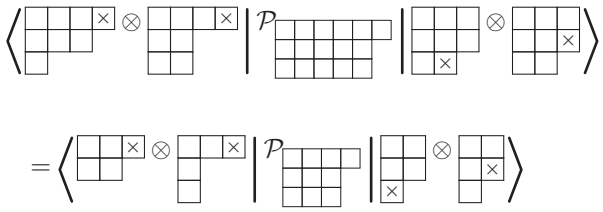

(25)

This also means that the number of such coefficients needed to implement our algorithm is finite: we calculate and store them before we actually start the simulation. But the number of such coefficients scales as $\sim M\,N^5$. First, there are M shapes

in the list (input of the algorithm), and for each of them there are at most N shapes which allow us to create sector γ_L. For instance, for $L = 8$, there are two nonvanishing entries per column in T_4[11]. More generally, this number scales as N. Then, for each of the four shapes appearing in the symbol, there are at most N bottom corners. For $N = 8$ and $M = 200$, MN^5 is already several million, so we also need an efficient algorithm to calculate those coefficients. We describe one of them below.

1. Application of Chen's method to calculate the subduction coefficients

In this section, we show how to calculate the coefficients $\langle\beta_{q_3},l_3| \otimes \langle\beta_{q_4},l_4|\mathcal{P}_{\gamma_L}|\beta_{q_1},l_1\rangle \otimes |\beta_{q_2},l_2\rangle$, where β_{q_j} is a shape [i.e., SU(N) irrep or Young diagram], and l_j is the row of the corresponding bottom corner (which satisfies $1 \leqslant l_j \leqslant N$ and which is enough to determine the exact location of the bottom corner inside β_{q_j}) for $j = 1,2,3,4$. We will assume that the conditions (1), (2), and (3) stated above are satisfied. We will describe in detail the different steps to calculate this kind of coefficient, and we will apply them to the SU(3) example introduced above [see Eq. (20)] in which $\beta_{q_1} = \beta_{q_2} = [2,2,1]$, $\beta_{q_3} = \beta_{q_4} = [3,2]$, $l_1 = l_2 = 3$, and $l_3 = l_4 = 1$, in order to prove Eq. (20). The idea is to use the SYTs and the orthogonal representation of the symmetric group to make this kind of calculation.

Step 1:

We first replace the couple (β_{q_1},l_1) by a SYT S_1 of the same shape, having its last number located in the bottom corner l_1: $(\beta_{q_1},l_1) \to S_1$. For our example, one can take, for instance,

$$\begin{array}{|c|c|}\hline &\\\hline &\\\hline \times&\\\cline{1-1}\end{array} \to \begin{array}{|c|c|}\hline 1&3\\\hline 2&4\\\hline 5\\\cline{1-1}\end{array} = S_1. \tag{26}$$

For the second couple (β_{q_2},l_2), we make a slightly different replacement: we replace the couple (β_2,l_2) by the SYT S_2^t which has shape β_2 and which is the last one in the last letter order (see the Appendix, Sec. A 2 for a definition), and we keep in memory the bottom corner l_2 for the next step. Then we reindex the numbers located in S_2^t to agree with the indexing in Fig. 1: $(1,2,\dots) \to (L,L-1,\dots)$ in order to obtain S_2. Thus, we have the transformation $(\beta_{q_2},l_2) \to S_2^t \to S_2$. For our example, one then has the following:

$$\begin{array}{|c|c|}\hline &\\\hline &\\\hline \times&\\\cline{1-1}\end{array} \to \begin{array}{|c|c|}\hline &\\\hline &\\\cline{1-2}\end{array} \to \begin{array}{|c|c|}\hline 1&4\\\hline 2&5\\\hline 3\\\cline{1-1}\end{array} \to \begin{array}{|c|c|}\hline 10&7\\\hline 9&6\\\hline 8\\\cline{1-1}\end{array} = S_2. \tag{27}$$

Step 2:

We then expand the "product" $S_1 \otimes S_2$ on the shape γ_L employing Chen's method, which makes use of the *permutational subduction coefficients* (see Sec. 4.18.3 in [33]). One must find a linear superposition of SYTs of shape γ_L having the same properties of "internal symmetries" between particles as the product $S_1 \otimes S_2$. For instance, the product

$$\begin{array}{|c|c|}\hline 1&3\\\hline 2&4\\\hline 5\\\cline{1-1}\end{array} \otimes \begin{array}{|c|c|}\hline 10&7\\\hline 9&6\\\hline 8\\\cline{1-1}\end{array} \tag{28}$$

is antisymmetric in the exchange $1 \leftrightarrow 2$, $6 \leftrightarrow 7$, and $9 \leftrightarrow 10$, since 1, 6, and 9 appear in the same column as 2, 7, and 10, respectively. Consequently, its development on γ_L should have a vanishing component on the following SYT of shape γ_L,

$$\begin{array}{|c|c|c|c|}\hline 1&2&7&10\\\hline 3&4&8\\\cline{1-3}5&6&9\\\cline{1-3}\end{array} \tag{29}$$

since this latter is symmetric in the exchange $1 \leftrightarrow 2$ and not antisymmetric. A systematic way to find the proper expansion with good coefficients is the following: We first create the $f^{\gamma_L}_{\beta_{q_1},\beta_{q_2}}$ SYTs of shape γ_L whose $L/2$ first entries are located at the same place as in S_1. Here, the $f^{\gamma_L}_{\beta_{q_1},\beta_{q_2}} = f^{[4,3,3]}_{[2,2,1],[2,2,1]} = 11$ SYTs are

$$\begin{array}{|c|c|c|c|}\hline 1&3&6&7\\\hline 2&4&8\\\cline{1-3}5&9&10\\\cline{1-3}\end{array}\quad \begin{array}{|c|c|c|c|}\hline 1&3&6&8\\\hline 2&4&7\\\cline{1-3}5&9&10\\\cline{1-3}\end{array}\quad \begin{array}{|c|c|c|c|}\hline 1&3&6&7\\\hline 2&4&9\\\cline{1-3}5&8&10\\\cline{1-3}\end{array}\quad \begin{array}{|c|c|c|c|}\hline 1&3&6&8\\\hline 2&4&9\\\cline{1-3}5&7&10\\\cline{1-3}\end{array}\quad \begin{array}{|c|c|c|c|}\hline 1&3&7&8\\\hline 2&4&9\\\cline{1-3}5&6&10\\\cline{1-3}\end{array}\quad \begin{array}{|c|c|c|c|}\hline 1&3&6&9\\\hline 2&4&8\\\cline{1-3}5&7&10\\\cline{1-3}\end{array}$$

$$\begin{array}{|c|c|c|c|}\hline 1&3&6&9\\\hline 2&4&8\\\cline{1-3}5&7&10\\\cline{1-3}\end{array}\quad \begin{array}{|c|c|c|c|}\hline 1&3&7&9\\\hline 2&4&8\\\cline{1-3}5&6&10\\\cline{1-3}\end{array}\quad \begin{array}{|c|c|c|c|}\hline 1&3&6&10\\\hline 2&4&7\\\cline{1-3}5&8&9\\\cline{1-3}\end{array}\quad \begin{array}{|c|c|c|c|}\hline 1&3&6&10\\\hline 2&4&8\\\cline{1-3}5&7&9\\\cline{1-3}\end{array}\quad \begin{array}{|c|c|c|c|}\hline 1&3&7&10\\\hline 2&4&8\\\cline{1-3}5&6&9\\\cline{1-3}\end{array} \tag{30}$$

Any combination of the last SYTs will have the same internal symmetry properties between the first $L/2$ entries as in S_1. To find the combination (written like a *ket* : $|\Phi^{S_1\otimes S_2}_{\gamma_L}\rangle$) which will have the same internal symmetry properties between the entries $L/2+1, L/2+2, \dots, L$ as in S_2, one needs now to use the following formula for the quadratic Casimir C^2, which holds for a general irrep $\beta = [\beta_1,\beta_2,\dots,\beta_k]$ with n boxes and $k \leqslant N$ rows:

$$C^2(\beta) = \sum_{1\leqslant i<j\leqslant n} P_{i,j} = \frac{1}{2}\left\{\sum_i \beta_i^2 - \sum_j \left(\beta_j^T\right)^2\right\}, \tag{31}$$

where β_i are the lengths of the rows, β_j^T are the lengths of the columns (which are also the rows of the transposed shape β^T), and $P_{i,j}$ are the permutations between indices i and j. Using the relevant indexing for S_2, we apply the formula (31) to the $L/2-1$ *successive* shapes which are made of 2, 3, $\dots$, $L/2$ boxes, which respectively contain the set of numbers $\{L,L-1\}$, $\{L,L-1,L-2\}$, and $\{L,L-1,\dots,L/2+1\}$, and that we write as $\beta_{q_2}(2),\beta_{q_2}(3),\dots,\beta_{q_2}(L/2)$, respectively. This chain of successive shapes allows one to reconstruct S_2. The application of the formula (31) to such a chain of shapes provides a set of $L/2-1$ equations that $|\Phi^{S_1\otimes S_2}_{\gamma_L}\rangle$ should satisfy. So, in our example, one has

(a) $P_{9,10}\left|\Phi^{S_1\otimes S_2}_{\gamma_L}\right\rangle = C^2([1,1])\left|\Phi^{S_1\otimes S_2}_{\gamma_L}\right\rangle = -\left|\Phi^{S_1\otimes S_2}_{\gamma_L}\right\rangle$,

since 9 and 10 appear in S_2 in the subshape $\begin{array}{|c|c|}\hline &\\\hline \\\cline{1-1}\end{array}$. (32)

(b) $(P_{9,10}+P_{8,10}+P_{8,9})|\Phi^{S_1\otimes S_2}_{\gamma_L}\rangle = C^2([1,1,1])|\Phi^{S_1\otimes S_2}_{\gamma_L}\rangle$
$= -3|\Phi^{S_1\otimes S_2}_{\gamma_L}\rangle$,

since 8, 9, and 10 appear in S_2 in the subshape $\begin{array}{|c|c|}\hline &\\\hline \\\cline{1-1}\\\cline{1-1}\end{array}$.

(c) $(P_{9,10}+P_{8,10}+P_{8,9}+P_{7,8}+P_{7,9}+P_{7,10})|\Phi^{S_1\otimes S_2}_{\gamma_L}\rangle$
$= C^2([2,1,1])|\Phi^{S_1\otimes S_2}_{\gamma_L}\rangle = -2|\Phi^{S_1\otimes S_2}_{\gamma_L}\rangle$,

since 7, 8, 9, and 10 appear in S_2 in the subshape $\begin{array}{|c|c|}\hline &\\\hline \\\cline{1-1}\\\cline{1-1}\end{array}$.

(d) $(P_{9,10}+P_{8,10}+P_{8,9}+P_{7,8}+P_{7,9}+P_{7,10}+P_{6,7}+P_{6,8}+P_{6,9}+P_{6,10})|\Phi_{\gamma_L}^{S_1\otimes S_2}\rangle = C^2([2,2,1])|\Phi_{\gamma_L}^{S_1\otimes S_2}\rangle = -2|\Phi_{\gamma_L}^{S_1\otimes S_2}\rangle$,

since 6, 7, 8, 9, and 10 appear in S_2 in the subshape $\begin{array}{|c|c|}\hline\multicolumn{1}{|c|}{}&\multicolumn{1}{|c|}{}\\\hline\multicolumn{1}{|c|}{}&\multicolumn{1}{|c|}{}\\\hline\multicolumn{1}{|c|}{}\\\cline{1-1}\end{array}$.

As long as γ_L appears in $\beta_{q_1}\otimes\beta_{q_2}$ with multiplicity 1 (the number of times that some irrep appears inside a tensor product is called the *outer multiplicity*), there is one and only one state $|\Phi_{\gamma_L}^{S_1\otimes S_2}\rangle$ (up to a phase) which satisfies the last $L/2-1$ equations simultaneously. This is always true in the system under investigation in the current article: the antiferromagnetic SU(N) Heisenberg model with one particle per site in the fundamental irrep, but not always true for the relevant physical problems, as we will discuss in the perspectives. From a practical point of view, one can transform the last problem into the quest of the unique null state of the operator:

$$\mathcal{C}_{S_2}=\sum_{q=2}^{L/2}\left\{\sum_{j=L-q+2}^{L}P_{L-q+1,j}-C^2(\beta_{q_2}(q))+C^2(\beta_{q_2}(q-1))\right\}^2, \tag{33}$$

expressed in the *basis* of the $f^{\gamma_L}_{\beta_{q_1},\beta_{q_2}}$ SYTs of shape γ_L with the first $L/2$ entries the same as in S_1. We use the rules of the orthogonal representation of the symmetric group to write the $f^{\gamma_L}_{\beta_{q_1},\beta_{q_2}}\times f^{\gamma_L}_{\beta_{q_1},\beta_{q_2}}$ matrix which represents such an operator on such a basis. For our example, the unique (up to a minus sign) normalized null state of the operator,

$$\begin{aligned}\mathcal{C}_{S_2}=&\{P_{9,10}+1\}^2+\{P_{8,10}+P_{8,9}+2\}^2\\&+\{P_{7,8}+P_{7,9}+P_{7,10}-1\}^2\\&+\{P_{6,7}+P_{6,8}+P_{6,9}+P_{6,10}\}^2,\end{aligned} \tag{34}$$

expressed in the basis shown in (30), is

$$|\Phi_{\gamma_L}^{S_1\otimes S_2}\rangle=\frac{2}{3}\begin{array}{|c|c|c|c|}\hline1&3&6&8\\\hline2&4&9\\\cline{1-3}5&7&10\\\cline{1-3}\end{array}+\frac{-\sqrt{2}}{3}\begin{array}{|c|c|c|c|}\hline1&3&7&8\\\hline2&4&9\\\cline{1-3}5&6&10\\\cline{1-3}\end{array}+\frac{\sqrt{2}}{3\sqrt{3}}\begin{array}{|c|c|c|c|}\hline1&3&6&10\\\hline2&4&8\\\cline{1-3}5&7&9\\\cline{1-3}\end{array}+\frac{\sqrt{2}}{3\sqrt{3}}\begin{array}{|c|c|c|c|}\hline1&3&7&9\\\hline2&4&8\\\cline{1-3}5&6&10\\\cline{1-3}\end{array}+\frac{-2}{3\sqrt{3}}\begin{array}{|c|c|c|c|}\hline1&3&6&9\\\hline2&4&8\\\cline{1-3}5&7&10\\\cline{1-3}\end{array}+\frac{-1}{3\sqrt{3}}\begin{array}{|c|c|c|c|}\hline1&3&7&10\\\hline2&4&8\\\cline{1-3}5&6&9\\\cline{1-3}\end{array}. \tag{35}$$

Since there is a freedom in the choice of a sign in the set of real coefficients in Eq. (35) (one can take $\pm|\Phi_{\gamma_L}^{S_1\otimes S_2}\rangle$), one can choose a convention: the coefficient of the first SYT (in the last letter order) in $|\Phi_{\gamma_L}^{S_1\otimes S_2}\rangle$ must be taken as positive [equal to 2/3 in Eq. (35)]. This kind of convention is important here because there are consistency relations between the different coefficients (and their different signs) that we are currently calculating. Step 3 is actually motivated by the same reason.

Step 3:

This stage is a bit technical and is only necessary if l_2 is not the highest possible bottom corner in β_{q_2}. It corresponds to the development around Eqs. (4-172) and (4-173) in [33]. The purpose of this stage is to act on $|\Phi_{\gamma_L}^{S_1\otimes S_2}\rangle$ with the sequence of permutational operations that would move the bottom corner in S_2 from its current location (which is the highest possible by construction) to l_2 in such a way that one would obtain S_2'. The SYT S_2' is defined as the SYT of shape β_{q_2}, with the number $L/2+1$ located in the bottom corner l_2 and with numbers $L/2+2, L/2+3,\ldots,L$ located in the shape $\beta_{q_2}(L/2-1)$ at some positions corresponding to the last SYT of shape $\beta_{q_2}(L/2-1)$ in the last letter order. The shape $\beta_{q_2}(L/2-1)$ is the shape β_{q_2} without the bottom corner located in l_2. In our example, one has

$$\text{For }(\beta_{q_2},l_2)=\begin{array}{|c|c|}\hline\multicolumn{1}{|c|}{}&\multicolumn{1}{|c|}{}\\\hline\multicolumn{1}{|c|}{}&\multicolumn{1}{|c|}{}\\\hline\multicolumn{1}{|c|}{\times}\\\cline{1-1}\end{array},\ S_2=\begin{array}{|c|c|c|}\hline10&7\\\hline9&6\\\cline{1-2}8\\\cline{1-1}\end{array}\ \text{and}\ \ S_2'=\begin{array}{|c|c|c|}\hline10&8\\\hline9&7\\\cline{1-2}6\\\cline{1-1}\end{array}. \tag{36}$$

In general, the sequence of operations $\mathcal{T}_{S_2}^{S_2'}$ that will transform S_2 into S_2' can be written as

$$\mathcal{T}_{S_2}^{S_2'}=\mathcal{T}_{\frac{L}{2}+2}\ldots\mathcal{T}_{k-1}\mathcal{T}_k, \tag{37}$$

where k is the largest integer belonging to $\{\frac{L}{2}+2,\frac{L}{2}+3,\ldots,L-1\}$ whose location in S_2 is different than its location in S_2', and where the operator that exchanges numbers q and $q-1$ $\mathcal{T}_q$ when acting on a given SYT S can be defined (for $q\geqslant 2$) as

$$\mathcal{T}_qS=\frac{P_{q-1,q}-\rho_{q-1,q}\mathcal{I}}{\sqrt{1-\rho_{q-1,q}^2}}S, \tag{38}$$

where $P_{q-1,q}$ is the permutation between numbers q and $q-1$, $\rho_{q-1,q}$ is the inverse of the axial distance between q and $q-1$ in the SYT S, and where $\mathcal{I}$ is the identity. This follows from the expression of the matrix describing permutations of consecutive numbers using SYTs (see Appendix). In our example, one has $k=8$, and

$$\begin{aligned}\mathcal{T}_{S_2}^{S_2'}S_2=\mathcal{T}_7\mathcal{T}_8S_2=\mathcal{T}_7\mathcal{T}_8\begin{array}{|c|c|c|}\hline10&7\\\hline9&6\\\cline{1-2}8\\\cline{1-1}\end{array}&=\mathcal{T}_7\frac{P_{7,8}-\rho_{7,8}\mathcal{I}}{\sqrt{1-\rho_{7,8}^2}}\begin{array}{|c|c|c|}\hline10&7\\\hline9&6\\\cline{1-2}8\\\cline{1-1}\end{array}\\&=\mathcal{T}_7\frac{P_{7,8}-\frac{1}{3}\mathcal{I}}{\sqrt{1-\frac{1}{9}}}\begin{array}{|c|c|c|}\hline10&7\\\hline9&6\\\cline{1-2}8\\\cline{1-1}\end{array}=\frac{P_{6,7}-\frac{1}{2}\mathcal{I}}{\sqrt{1-\frac{1}{4}}}\begin{array}{|c|c|c|}\hline10&8\\\hline9&6\\\cline{1-2}7\\\cline{1-1}\end{array}=\begin{array}{|c|c|c|}\hline10&8\\\hline9&7\\\cline{1-2}6\\\cline{1-1}\end{array}=S_2'.\end{aligned} \tag{39}$$

We then act with $\mathcal{T}_{S_2}^{S_2'}$ on $|\Phi_{\gamma_L}^{S_1\otimes S_2}\rangle$ to obtain $|\Phi_{\gamma_L}^{S_1\otimes S_2'}\rangle$; here, using Eq. (39), Eq. (35), and the rules for the orthogonal representation of the symmetric group, we get

$$\begin{aligned}\mathcal{T}_{S_2}^{S_2'}|\Phi_{\gamma_L}^{S_1\otimes S_2}\rangle=\frac{P_{6,7}-\frac{1}{2}\mathcal{I}}{\sqrt{1-\frac{1}{4}}}\times\frac{P_{7,8}-\frac{1}{3}\mathcal{I}}{\sqrt{1-\frac{1}{9}}}|\Phi_{\gamma_L}^{S_1\otimes S_2}\rangle&\\=|\Phi_{\gamma_L}^{S_1\otimes S_2'}\rangle=\frac{1}{4}\begin{array}{|c|c|c|c|}\hline1&3&6&10\\\hline2&4&8\\\cline{1-3}5&7&9\\\cline{1-3}\end{array}+\frac{-\sqrt{3}}{4}\begin{array}{|c|c|c|c|}\hline1&3&6&10\\\hline2&4&7\\\cline{1-3}5&8&9\\\cline{1-3}\end{array}+\frac{\sqrt{3}}{2\sqrt{2}}\begin{array}{|c|c|c|c|}\hline1&3&6&9\\\hline2&4&7\\\cline{1-3}5&8&10\\\cline{1-3}\end{array}+\frac{-1}{2\sqrt{2}}\begin{array}{|c|c|c|c|}\hline1&3&6&9\\\hline2&4&8\\\cline{1-3}5&7&10\\\cline{1-3}\end{array}&\\+\frac{-\sqrt{3}}{4\sqrt{2}}\begin{array}{|c|c|c|c|}\hline1&3&6&8\\\hline2&4&9\\\cline{1-3}5&7&10\\\cline{1-3}\end{array}+\frac{\sqrt{5}}{4\sqrt{2}}\begin{array}{|c|c|c|c|}\hline1&3&6&7\\\hline2&4&9\\\cline{1-3}5&8&10\\\cline{1-3}\end{array}.&\end{aligned} \tag{40}$$

The coefficients appearing in the right-hand side of Eqs. (35) and (40) are the $S_L \subset S_{\frac{L}{2}} \otimes S_{\frac{L}{2}}$ *subduction coefficients* [33], where S_n stands for the symmetric group of n elements.

Now, one can wonder why we have not taken directly S_2' at then end of step 1 in order to start step 2 with the expansion of the product $S_1 \otimes S_2'$ and not $S_1 \otimes S_2$. If we did so, we would obtain in general the same combination as $|\Phi_{\gamma_L}^{S_1 \otimes S_2'}\rangle$ up to a sign. To ensure some consistency relations between subduction coefficients, as first pointed out by Chen [33], one needs to start doing calculation on S_2, the *last* SYT of shape β_{q_2}. Let us stress that these signs are not just a matter of convention. It is absolutely necessary to keep track of them to get the matrix right.

Steps 4, 5, & 6:

We perform steps 1, 2, and 3 but with (β_{q_3}, l_3) instead of (β_{q_1}, l_1), and (β_{q_4}, l_4) instead of (β_{q_2}, l_2). In our example, we have

$$S_3 = \begin{array}{|c|c|c|}\hline 1&3&5\\\hline 2&4\\\cline{1-2}\end{array} \text{ and } S_4 = S_4' = \begin{array}{|c|c|c|}\hline 10&8&6\\\hline 9&7\\\cline{1-2}\end{array}, \tag{41}$$

and

$$|\Phi_{\gamma_L}^{S_3 \otimes S_4'}\rangle = \frac{1}{4}\begin{array}{|c|c|c|c|}\hline 1&3&5&10\\\hline 2&4&8\\\cline{1-3}6&7&9\\\cline{1-3}\end{array} + \frac{-\sqrt{3}}{4}\begin{array}{|c|c|c|c|}\hline 1&3&5&10\\\hline 2&4&7\\\cline{1-3}6&8&9\\\cline{1-3}\end{array} + \frac{\sqrt{3}}{2\sqrt{2}}\begin{array}{|c|c|c|c|}\hline 1&3&5&9\\\hline 2&4&7\\\cline{1-3}6&8&10\\\cline{1-3}\end{array}$$
$$+\frac{-1}{2\sqrt{2}}\begin{array}{|c|c|c|c|}\hline 1&3&5&9\\\hline 2&4&8\\\cline{1-3}6&7&10\\\cline{1-3}\end{array} + \frac{-\sqrt{3}}{4\sqrt{2}}\begin{array}{|c|c|c|c|}\hline 1&3&5&8\\\hline 2&4&9\\\cline{1-3}6&7&10\\\cline{1-3}\end{array} + \frac{\sqrt{5}}{4\sqrt{2}}\begin{array}{|c|c|c|c|}\hline 1&3&5&7\\\hline 2&4&9\\\cline{1-3}6&8&10\\\cline{1-3}\end{array}. \tag{42}$$

In our example, the coefficients in $|\Phi_{\gamma_L}^{S_1 \otimes S_2'}\rangle$ [Eq. (40)] are the same as in $|\Phi_{\gamma_L}^{S_3 \otimes S_4'}\rangle$ [Eq. (42)]; of course, this is not always true.

Step 7:

We finally use Young's rules (see Sec. A 2) to calculate

$$\langle \beta_{q_3}, l_3| \otimes \langle \beta_{q_4}, l_4|\mathcal{P}_{\gamma_L}|\beta_{q_1}, l_1\rangle \otimes |\beta_{q_2}, l_2\rangle = \left\langle \Phi_{\gamma_L}^{S_3 \otimes S_4'}|P_{\frac{L}{2},\frac{L}{2}+1}|\Phi_{\gamma_L}^{S_1 \otimes S_2'}\right\rangle. \tag{43}$$

In our example, we obtain

$$\left\langle \Phi_{\gamma_L}^{S_3 \otimes S_4'}|P_{\frac{L}{2},\frac{L}{2}+1}|\Phi_{\gamma_L}^{S_1 \otimes S_2'}\right\rangle = \frac{\sqrt{15}}{4}. \tag{44}$$

2. *Improvement of Chen's method: Taking a "shortcut" in the chain of subshapes*

The method developed in the last section is already quite powerful and would enable us to have accurate DMRG simulations for $N = 3$ or $N = 4$. However, when N increases, it becomes limited due to the high value of $f_{\beta_{q_1},\beta_{q_2}}^{\gamma_L}$, which determines the size of the matrix to obtain the unique null state of step 2. We found a way to greatly improve step 2 by taking advantage of the *Lego-like* structure of SU(N) irreps and SYTs. In fact, every shape or SYT with n boxes can either be seen as living in the tensor product of n fundamental irreps or as living in the tensor product of nonfundamental irreps, such as one-column fully antisymmetric irreps, for instance. Based on this principle, our method below is presented, which will lead to an important reduction of the size of the matrix to obtain the null state of step 2. For instance, for SU(6), and for $\beta_{q_1} = [4,3,3,2,2,2]$, $\beta_{q_2} = [3,3,3,3,3,1]$, there are $f_{\beta_{q_1},\beta_{q_2}}^{\gamma_L} = 1\,081\,080$ SYTs of shape $\gamma_L = [6,6,5,5,5,5]$, involving the necessity to find the null state of a matrix of size $1\,081\,080 \times 1\,081\,080$, while the matrix that we need to find the null state of in the current section has dimension 2×2. In this new example, one has (for $l_1 = 6$),

$$S_1 = \begin{array}{|c|c|c|c|}\hline 1&7&12&15\\\hline 2&8&13\\\cline{1-3}3&9&14\\\cline{1-3}4&10\\\cline{1-2}5&11\\\cline{1-2}6&16\\\cline{1-2}\end{array} \text{ and } S_2 = \begin{array}{|c|c|c|}\hline 32&26&21\\\hline 31&25&20\\\hline 30&24&19\\\hline 29&23&18\\\hline 28&22&17\\\hline 27\\\cline{1-1}\end{array}. \tag{45}$$

In Chen's method, S_2 would be characterized by the chain of successive subshapes containing the set of numbers $\{L, L-1\}, \{L, L-1, L-2\}, \{L, L-1, L-3,\}, \{L, L-1, L-2, \ldots, L/2+1\}$. In the current example, it would be

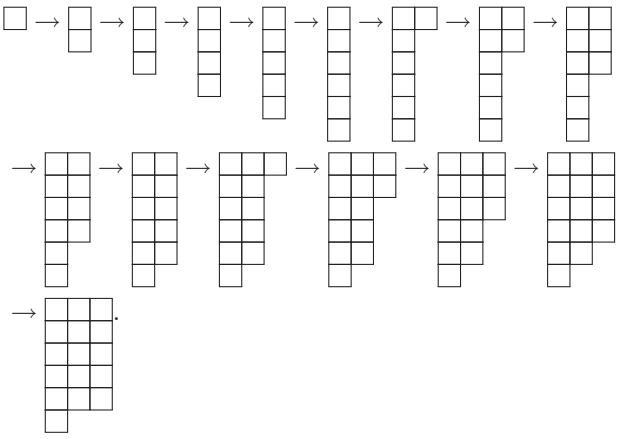

(46)

Then, from this chain we would build the operator $\mathcal{C}_{S_2}$ defined in Eq. (33). We would then look for the unique combination of SYTs of shape γ_L, null on $\mathcal{C}_{S_2}$ and built from the tensor product of $S_1 \in \beta_{q_1}$ and

$$S_2 \in \beta_{q_2} \in \square^{\otimes \frac{L}{2}}. \tag{47}$$

In the present section, we characterize S_2 by the chain of subshapes containing the set of numbers $\{L, L-1, L-2, \ldots, L+1-\beta_{q_2}^{T,1}\}$, $\{L, L-1, L-2, \ldots, L+1-\beta_{q_2}^{T,1}, L-\beta_{q_2}^{T,1}, \ldots, L-\beta_{q_2}^{T,1}-\beta_{q_2}^{T,2}+1,\}, \ldots, \{L, L-1, L-2, \ldots, L/2+1\}$, where the numbers $\beta_{q_2}^{T,j}$ stand for the length of the jth column in β_{q_2}, for $j = 1, \ldots, n_{\beta_{q_2}}^c$, with $n_{\beta_{q_2}}^c$ the number of columns in the shape β_{q_2}. In the current example, it is the chain

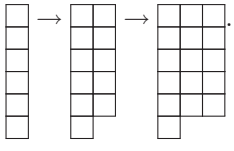

(48)

We will then look for all the states that live in the irrep represented by the shape γ_L and which are built from the tensor

product of the state $S_1 \in \beta_{q_1}$ and the states

$$S_2 \in \beta_{q_2} \in \begin{array}{|c|}\hline\\\hline\\\hline\\\hline\end{array} \otimes \begin{array}{|c|}\hline\\\hline\end{array} \otimes \ldots \otimes \begin{array}{|c|}\hline\\\hline\end{array}, \tag{49}$$

which means that β_{q_2} is now seen as an irrep produced by the tensor product of the one-column irreps of length $\beta_{q_2}^{T,k}$ from $k=1$ to $k=n_{\beta_{q_2}}^c$. These states are superpositions of SYTs of shape γ_L, which all have their first $L/2$ entries located as in S_1, and their entries $\{L/2+1, L/2+2, \ldots, L\}$ which satisfy some internal constraints corresponding to the product of $n_{\beta_{q_2}}^c$ fully antisymmetric irreps of length $\beta_{q_2}^{T,k}$ from $k=1$ to $k=n_{\beta_{q_2}}^c$. Such a set of internal constraints for the case of an antisymmetric irrep was first pointed out in Ref. [17]. Let us call $\mathrm{Col}_k^{S_2}$ the set of numbers located in the kth column of S_2 (for $k=1,\ldots,n_{\beta_{q_2}}^c$). The internal constraints here are the following: Every SYT should be such that the set of decreasing numbers belonging to $\mathrm{Col}_k^{S_2}$ must appear in the shape γ_L in strictly ascending rows from bottom to top, for $k=1,\ldots,n_{\beta_{q_2}}^c$. The number of such SYTs will be named $\tilde{f}_{\beta_{q_1},\beta_{q_2}}^{\gamma_L}$ and is often much smaller than $f_{\beta_{q_1},\beta_{q_2}}^{\gamma_L}$. In our example, $\tilde{f}_{\beta_{q_1},\beta_{q_2}}^{\gamma_L}=2$, and the 2 SYTs which satisfy all the constraints are

$$\tilde{S}_{\beta_{q_1},\beta_{q_2}}^{\gamma_L,1} = \begin{array}{|c|c|c|c|c|c|}\hline 1&7&12&15&22&27\\\hline 2&8&13&17&23&28\\\hline 3&9&14&18&29\\\cline{1-5} 4&10&19&24&30\\\cline{1-5} 5&11&20&25&31\\\cline{1-5} 6&16&21&26&32\\\cline{1-5}\end{array},$$

$$\tilde{S}_{\beta_{q_1},\beta_{q_2}}^{\gamma_L,2} = \begin{array}{|c|c|c|c|c|c|}\hline 1&7&12&15&17&27\\\hline 2&8&13&18&22&28\\\hline 3&9&14&23&29\\\cline{1-5} 4&10&19&24&30\\\cline{1-5} 5&11&20&25&31\\\cline{1-5} 6&16&21&26&32\\\cline{1-5}\end{array}, \tag{50}$$

where for instance, one can check that the set of numbers $\mathrm{Col}_1^{S_2}=\{32,31,30,\ldots,27\}$ which appears in the first column of S_2 in Eq. (45) are located in the two SYTs of Eq. (50) in strictly ascending rows from 32 to 27. Using the words and concepts developed in [17,18], these two SYTs must be seen as *representatives* of *equivalence classes*. The SYT $\tilde{S}_{\beta_{q_1},\beta_{q_2}}^{\gamma_L,j}$ (for some j such that $1 \leqslant j \leqslant \tilde{f}_{\beta_{q_1},\beta_{q_2}}^{\gamma_L}$) represents all the SYTs of the same shape γ_L, with entries from 1 to $L/2$ at the same location as in S_1 and with entries from $L/2+1$ to L being at the same location as in $\tilde{S}_{\beta_{q_1},\beta_{q_2}}^{\gamma_L,j}$ up to some permutation among the numbers along each column in S_2. For instance, the SYTs

$$\begin{array}{|c|c|c|c|c|c|}\hline 1&7&12&15&22&27\\\hline 2&8&13&17&24&29\\\hline 3&9&14&18&28\\\cline{1-5} 4&10&19&23&30\\\cline{1-5} 5&11&20&25&31\\\cline{1-5} 6&16&21&26&32\\\cline{1-5}\end{array}, \quad \begin{array}{|c|c|c|c|c|c|}\hline 1&7&12&15&22&29\\\hline 2&8&13&17&23&30\\\hline 3&9&14&18&27\\\cline{1-5} 4&10&19&24&28\\\cline{1-5} 5&11&20&25&31\\\cline{1-5} 6&16&21&26&32\\\cline{1-5}\end{array} \text{ and } \begin{array}{|c|c|c|c|c|c|}\hline 1&7&12&15&22&29\\\hline 2&8&13&19&23&30\\\hline 3&9&14&20&27\\\cline{1-5} 4&10&17&24&28\\\cline{1-5} 5&11&18&25&31\\\cline{1-5} 6&16&21&26&32\\\cline{1-5}\end{array} \tag{51}$$

are three SYTs (among many others) which belong to the equivalence class represented by the SYT $\tilde{S}_{\beta_{q_1},\beta_{q_2}}^{\gamma_L,1}$ appearing in Eq. (50). From each SYT $\tilde{S}_{\beta_{q_1},\beta_{q_2}}^{\gamma_L,j}$ (for j such that $1 \leqslant j \leqslant \tilde{f}_{\beta_{q_1},\beta_{q_2}}^{\gamma_L}$), we then construct a *state* $|\tilde{\phi}_{\beta_{q_1},\beta_{q_2}}^{\gamma_L,j}\rangle$, which is a linear combination of SYTs belonging to the same class, obtained by using some projection operator [17,18] that ensures the property of antisymmetry among the numbers located in each column of S_2: $|\tilde{\phi}_{\beta_{q_1},\beta_{q_2}}^{\gamma_L,j}\rangle = \mathcal{N}^{-1} Proj \tilde{S}_{\beta_{q_1},\beta_{q_2}}^{\gamma_L,j}$.

We then define a new operator $\tilde{\mathcal{C}}_{S_2}$ as

$$\tilde{\mathcal{C}}_{S_2} = \sum_{k=1}^{n_{\beta_{q_2}}^c-1} \left\{ P_{n_k^{S_2},n_k^{S_2}-1} - \frac{1}{\beta_{q_2}^{T,k}} \right\}^2, \tag{52}$$

where the number $n_k^{S_2} = L+1-\sum_{r=1}^{k}\beta_{q_2}^{T,k}$ (for $k=1,\ldots,n_{\beta_{q_2}}^c$) is the number located in the last row of the kth column in S_2. In our example, $\tilde{\mathcal{C}}_{S_2}$ would be

$$\tilde{\mathcal{C}}_{S_2} = \left\{ P_{26,27} - \frac{1}{6} \right\}^2 + \left\{ P_{21,22} - \frac{1}{5} \right\}^2. \tag{53}$$

The state $|\Phi_{\gamma_L}^{S_1\otimes S_2}\rangle$ (which was defined in the previous section) can be obtained by looking for the (unique) null state of $\tilde{\mathcal{C}}_{S_2}$ expressed in the *basis* of states $|\tilde{\phi}_{\beta_{q_1},\beta_{q_2}}^{\gamma_L,j}\rangle$. To prove such a claim, we use the formula (31) applied on the subshape made of the kth column in S_2 (of length $\beta_{q_2}^{T,k}$) and the highest box of the $(k+1)$th column of S_2 (for $k=1,\ldots,n_{\beta_{q_2}}^c-1$), which is filled by the set of consecutive numbers $\mathrm{Col}_k^{S_2}\cup\{n_k^{S_2}-1\} = \{n_k^{S_2}+\beta_{q_2}^{T,k}-1, n_k^{S_2}+\beta_{q_2}^{T,k}-2,\ldots,n_k^{S_2},n_k^{S_2}-1\}$:

$$\sum_{\substack{i,j\in \mathrm{Col}_k^{S_2}\cup\{n_k^{S_2}-1\}\\ i<j}} P_{i,j}\left|\Phi_{\gamma_L}^{S_1\otimes S_2}\right\rangle = \left\{1+\beta_{q_2}^{T,k}\frac{1-\beta_{q_2}^{T,k}}{2}\right\}\left|\Phi_{\gamma_L}^{S_1\otimes S_2}\right\rangle$$

since $\mathrm{Col}_k^{S_2}\cup\{n_k^{S_2}-1\}$ appear in S_2 in the subshape:

$$\overset{\beta_{q_2}^{T,k}}{\left\{\vphantom{\begin{array}{|c|}\hline\\\hline\\\hline\end{array}}\right.}\begin{array}{|c|c|}\hline\\\hline\\\hline\\\cline{1-1}\end{array}. \tag{54}$$

Now, since

$$\sum_{\substack{i,j\in \mathrm{Col}_k^{S_2}\cup\{n_k^{S_2}-1\}\\ i<j}} P_{i,j} = \sum_{\substack{i\in \mathrm{Col}_k^{S_2}\\ j=n_k^{S_2}-1}} P_{i,j} + \sum_{\substack{i,j\in \mathrm{Col}_k^{S_2}\\ i<j}} P_{i,j} \tag{55}$$

and since $|\Phi_{\gamma_L}^{S_1\otimes S_2}\rangle$ should be fully antisymmetric in the exchange $i \leftrightarrow j$, where $i,j \in \mathrm{Col}_k^{S_2}$, one should have

$$\sum_{\substack{i\in \mathrm{Col}_k^{S_2}\\ j=n_k^{S_2}-1}} P_{i,j}|\Phi_{\gamma_L}^{S_1\otimes S_2}\rangle = |\Phi_{\gamma_L}^{S_1\otimes S_2}\rangle. \tag{56}$$

Second, if we also use the antisymmetry for the numbers inside $\mathrm{Col}_{k+1}^{S_2}$, and if we write $P_{i,j} = P_{j,n_k^{S_2}-1}P_{i,n_k^{S_2}-1}P_{j,n_k^{S_2}-1}$ for $i \in$

$\mathrm{Col}_k^{S_2}$ and for $j \in \mathrm{Col}_{k+1}^{S_2}$, we obtain, $\forall k = 1,\ldots,n^c_{\beta_{q_2}} - 1$:

$$H^{\mathrm{Col},S_2}_{k,k+1}|\Phi^{S_1\otimes S_2}_{\gamma_L}\rangle = \sum_{\substack{i\in \mathrm{Col}_k^{S_2}\\ j\in \mathrm{Col}_{k+1}^{S_2}}} P_{i,j}|\Phi^{S_1\otimes S_2}_{\gamma_L}\rangle = \beta_{q_2}^{T,k+1}|\Phi^{S_1\otimes S_2}_{\gamma_L}\rangle, \tag{57}$$

where we have also defined $H^{\mathrm{Col},S_2}_{k,k+1}$ as the sum of $\beta_{q_2}^{T,k+1}\times\beta_{q_2}^{T,k}$ permutations $P_{i,j}$ that interexchange numbers $i \in \mathrm{Col}_k^{S_2}$ with numbers $j \in \mathrm{Col}_{k+1}^{S_2}$. This set of $n^c_{\beta_{q_2}} - 1$ equations [Eq. (57)] now replaces the set of $L/2-1$ equations appearing in Eq. (32) for the case treated using Chen's method. It should be solved in the basis of states $\{|\tilde{\phi}^{\gamma_L,m}_{\beta_{q_1},\beta_{q_2}}\rangle, m = 1,\ldots,\tilde{f}^{\gamma_L}_{\beta_{q_1},\beta_{q_2}}\}$ which are antisymmetric on each set of numbers $\mathrm{Col}_k^{S_2}$ (for $k = 1,\ldots,n^c_{\beta_{q_2}}$) by construction. This set of equations uniquely determines $|\Phi^{S_1\otimes S_2}_{\gamma_L}\rangle$. Finally, the null state of

$$\sum_{k=1}^{n^c_{\beta_{q_2}}-1}\left\{H^{\mathrm{Col},S_2}_{k,k+1} - \beta_{q_2}^{T,k+1}\right\}^2 \tag{58}$$

on the basis $\{|\tilde{\phi}^{\gamma_L,m}_{\beta_{q_1},\beta_{q_2}}\rangle, m = 1,\ldots,\tilde{f}^{\gamma_L}_{\beta_{q_1},\beta_{q_2}}\}$ is also the null state of $\tilde{\mathcal{C}}_{S_2}$ on such a basis since we have

$$\begin{aligned}&\langle\tilde{\phi}^{\gamma_L,m'}_{\beta_{q_1},\beta_{q_2}}|H^{\mathrm{Col},S_2}_{k,k+1}|\tilde{\phi}^{\gamma_L,m}_{\beta_{q_1},\beta_{q_2}}\rangle\\ &= \beta_{q_2}^{T,k+1}\beta_{q_2}^{T,k}\langle\tilde{\phi}^{\gamma_L,m'}_{\beta_{q_1},\beta_{q_2}}|P_{n_k^{S_2},n_k^{S_2}+1}|\tilde{\phi}^{\gamma_L,m}_{\beta_{q_1},\beta_{q_2}}\rangle,\end{aligned} \tag{59}$$

thanks also to the antisymmetry in $\mathrm{Col}_k^{S_2}$ and $\mathrm{Col}_{k+1}^{S_2}$. Note that if $\tilde{f}^{\gamma_L}_{\beta_{q_1},\beta_{q_2}} = 1$, one does not need to create $\tilde{\mathcal{C}}_{S_2}$ because one will directly have $|\Phi^{S_1\otimes S_2}_{\gamma_L}\rangle = |\tilde{\phi}^{\gamma_L,1}_{\beta_{q_1},\beta_{q_2}}\rangle$. Such a case occurs, for instance, when the shape β_{q_2} has only one column. Finally, from the coefficients of the null state of $\tilde{\mathcal{C}}_{S_2}$ and from the developments of the states $\{|\tilde{\phi}^{\gamma_L,m}_{\beta_{q_1},\beta_{q_2}}\rangle, m = 1,\ldots,\tilde{f}^{\gamma_L}_{\beta_{q_1},\beta_{q_2}}\}$, one recovers the subduction coefficients the way they would appear at the end of step 2. But the computation is much faster.

III. BETHE ANSATZ EQUATIONS FOR THE HEISENBERG SU(N) CHAIN WITH OPEN BOUNDARY CONDITIONS

In order to benchmark our DMRG code, we need to compare our numerical results to some exact results. The set of Bethe ansatz equations for a SU(N) Heisenberg chain of L sites with periodic boundary conditions (PBC) appears explicitly in Eq. (5.2 b) of [34]. Such a set of equations has been used by Alcaraz and Martins in [35] to obtain, among other results, the finite-size ring ground-state energies for the SU(3) and SU(4) Heisenberg chain with the fundamental irrep at each site.

Many interesting studies on the integrable SU(N) Heisenberg chains with different boundary conditions (and different irreps at each site) have been done in the past [36–38]; however, we have not been able to find in the literature the Bethe ansatz equations (BAE) for open boundary conditions (OBC) and the fundamental irrep in an explicit form that would be as simple to use as that of Eq. (5.2 b) in [34] (which is valid only for PBC), with the noticeable exception of a recent study of the SU(3) case [39]. So, as a first step, we write below the set of BAE for an L site SU(N) Heisenberg chain with OBC with the fundamental irrep at each site for general N:

$$\begin{aligned}&\arctan\left(2x_k^{(r)}\right) + \sum_{\alpha=r\pm1}\sum_{j=1}^{M^{(\alpha)}}\left\{\arctan\left(2\left[x_k^{(r)} - x_j^{(\alpha)}\right]\right)\right.\\ &\quad\left. + \arctan\left(2\left[x_k^{(r)} + x_j^{(\alpha)}\right]\right)\right\}\\ &\quad - \sum_{j=1}^{M^{(r)}}\left\{\arctan\left(x_k^{(r)} - x_j^{(r)}\right) + \arctan\left(x_k^{(r)} + x_j^{(r)}\right)\right\}\\ &= \pi I_k^{(r)}, \quad k = 1,\ldots,M^{(r)},\end{aligned} \tag{60}$$

for $r = 1,\ldots,N-1$. For the ground state, the quantum numbers $M^{(r)}$ and $I_k^{(r)}$ are integers given by

$$M^{(r)} = \mathrm{Floor}\left[L\left(1 - \frac{r}{N}\right)\right], \tag{61}$$

$$I_k^{(r)} = k, \ \text{for}\ k = 1,2,\ldots,M^{(r)}, \tag{62}$$

for $r = 1,\ldots,N-1$, while $M^{(N)} = 0$ and $M^{(0)} = L$. Finally, one should take $x_j^{(0)} = 0\ \forall j = 1,\ldots,L = M^{(0)}$. So, for instance, for $L = 12$ and SU(3), $M^{(1)} = 8$, $M^{(2)} = 4$, so that there are 12 unknown *Bethe roots* $\{x_k^{(r)}\}$, $(r = 1,2)$ that one can obtain numerically by solving the system of equations, Eq. (60).

Once the Bethe roots $x_l^{(1)}$ for $l = 1..M^{(1)}$ have been determined, the ground-state energy of the open chain of L sites can be obtained as

$$E(L) = -\sum_{l=1}^{M^{(1)}}\frac{1}{\frac{1}{4} + (x_l^{(1)})^2} + (L-1). \tag{63}$$

TABLE I. Exact ground-state energy per site of the SU(N) Heisenberg chain with the fundamental irrep at each site with open boundary conditions as a function of the length L, obtained by solving the Bethe ansatz equations of Eq. (60). For $L = \infty$, we took the formula from [40].

L	SU(3)	SU(4)	SU(5)	SU(6)	SU(8)
24	–0.69526268730064	–0.80982320364497	–0.86314662529649	–0.89518774036919	–0.92557160315540
60	–0.6998571791373	–0.8188090258187	–0.8765610853081	–0.9088545631758	–0.941247635.....[a]
120	–0.7015028275085	–0.8219288297026	–0.8806084906635	–0.9135413831900	–0.9472288106736
240	–0.7023491359327	–0.8235146373945	–0.8826593378956	–0.9159126071869	–0.9500136623979
600	–0.7028648366299	–0.8244749117138	–0.8838991109256	–0.9173448863563	–0.9516943959573
∞	–0.7032120767462	–0.8251189342374	–0.8847296926763	–0.9183039468245	–0.9528192495986

[a]There are fewer digits because the convergence of the numerical solver is not as good when L is not a multiple of N, for L larger than 40 typically.

In Table I, we list for some values of L and N the ground-state energy per site $E(L)/L$. For $L = 24$, and for smaller sizes not shown in the table, we have checked that they perfectly agree up to 14 digits and for all values of N with the energies obtained by Lanczos diagonalization using the algorithm of Ref. [16]. The values in Table I will be used in the next section to benchmark our DMRG code.

IV. DMRG RESULTS FOR THE SU(N) HEISENBERG CHAIN WITH OPEN BOUNDARY CONDITIONS

We have numerically investigated the Heisenberg SU(N) chain with OBC with our DMRG algorithm for $N = 3,4,5,6,$ and 8. We have performed the infinite-size DMRG until the desired length of the chain L was reached, and then we have performed some sweeps from left to right and from right to left through the finite-size DMRG. The implementation of the SU(N) symmetry in the finite-size DMRG involves exactly the same steps as in the infinite part, except that the left and the right blocks now have different sizes. In particular, the calculation of the matrix elements of the interaction term between the two blocks will depend on the $S_L \subset S_x \otimes S_{L-x}$ *subduction coefficients* [33], where x is the length of the left block. These coefficients are computed using the very same method as that developed in the previous part for the $S_L \subset S_{\frac{L}{2}} \otimes S_{\frac{L}{2}}$ *subduction coefficients*. We have computed the ground-state energies $\mathcal{E}_L$ at the end of the infinite-size DMRG and calculated the difference Δ_E^∞ with respect to the exact energies (shown in Table I). We have also calculated the ground-state energy during the finite-size part of the DMRG. We have noticed that after two sweeps, $\mathcal{E}_L$ starts saturating. The corresponding difference with the exact energy, named $\Delta_E^{\rm Sw}$, is typically 1–2 orders of magnitude smaller than Δ_E^∞. We list the results in Table II for $L = 120$ and for $L = 240$. Note that similar comparisons have been performed for SU(N) Hubbard chains, for which the Bethe ansatz is only approximate as soon as $N > 2$ [41].

During the sweeps, we have also computed the entanglement entropy $S(x)$ [see Eq. (15)] as a function of x, the position of the sweep (also the size of the left block). For critical spin chains with OBC, the entanglement entropy is given by the

TABLE II. DMRG results for a chain of $L = 120$ sites (third and fourth column) and of $L = 240$ sites (fifth and sixth column) with open boundary conditions. M is the number of irreps kept (see Sec. II A for details), Δ_E^∞ is the difference between the ground-state energy $\mathcal{E}_L$ obtained at the end of the infinite-size part of the DMRG, and the exact Bethe ansatz energies $E(L)$ (shown in Table I). $\Delta_E^{\rm Sw}$ corresponds to the same quantity after two sweeps, where $\mathcal{E}_L$ starts saturating. We have kept $m = 1000$ states for $L = 120$ and $m = 2000$ states for $L = 240$. Seventh column: discarded weight $\mathcal{W}_d^{120}$ at the end of the infinite-size DMRG for $L = 120$ and $m = 1000$.

N	M	$\Delta_E^\infty(120)$	$\Delta_E^{\rm Sw}(120)$	$\Delta_E^\infty(240)$	$\Delta_E^{\rm Sw}(240)$	$\mathcal{W}_d^{120}$
3	85	6×10^{-11}	6×10^{-13}	5×10^{-11}	8×10^{-13}	9×10^{-12}
4	160	4×10^{-9}	3×10^{-10}	3×10^{-9}	5×10^{-10}	6×10^{-9}
5	150	1×10^{-7}	4×10^{-9}	3×10^{-8}	8×10^{-9}	1×10^{-7}
6	150	1×10^{-7}	1×10^{-8}	9×10^{-8}	3×10^{-9}	2×10^{-5}
8	200	9×10^{-7}	7×10^{-7}	4×10^{-6}	4×10^{-6}	2×10^{-4}

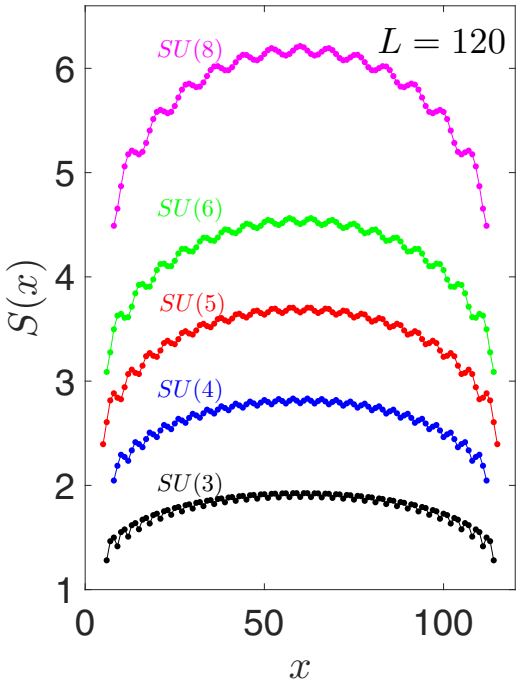

FIG. 8. Entanglement entropy $S(x)$ as a function of the position x along an open chain of $L = 120$ sites. The curves exhibit some N-periodic Friedel oscillations.

Calabrese-Cardy formula [42]:

$$S(x) = \frac{c}{6}\log\left[\frac{2L}{\pi}\sin\left(\frac{\pi x}{L}\right)\right] + K, \tag{64}$$

where K is a nonuniversal constant, and c is the central charge of the associated CFT. In the case of the Heisenberg SU(N) spin chains with the fundamental irrep at each site, the CFT is a Wess- Zumino-Witten (WZW) model with topological coupling $k = 1$ [SU(N)$_1$ WZW], with central charge $c_{\rm th} = N - 1$. We show in Fig. 8 the profile of the entanglement entropy $S(x)$ for $L = 120$ as a function of the position x. Because of the OBC, $S(x)$ has Friedel oscillation with N-fold periodicity. In order to remove the oscillations and to fit the central charge, we have adopted two strategies, illustrated in Fig. 9, where we analyze the case of SU(4), $L = 240$. Since the oscillations are N periodic, one can plot $S(x)$ as a function of the logarithm of the conformal distance $\frac{1}{6}\log[\frac{2L}{\pi}\sin(\frac{\pi x}{L})]$ separately for different sets of abscissa x of the form $x = N \times p + q$. Each set corresponds to a fixed $q = 0,1,..N-1$ and to all values of p consistent with the overall length. It then gives rise to N different straight lines (one for each q), as shown in top of Fig. 9, with different slopes c_q. It turns out that one always has $c_{N/2} \leqslant ... \leqslant c_0$. In particular, fitting $S(x)$ for x multiple of N always gives rise to the largest central charge, while fitting $S(x)$ for $x \equiv N/2 \bmod N$ always gives the smallest one. Note that when N is odd, $N/2$ should be understood as Floor($N/2$). Alternatively, one can also follow the strategy developed in [43]. Since the Friedel oscillations originate from the bond modulations, it is convenient to introduce $\tilde{S}_k(x) = S(x) + k\langle P_{x,x+1}\rangle$, where $\langle P_{x,x+1}\rangle$ is the expectation value on the ground state of the bond operator $P_{x,x+1}$, and where k is a parameter that is adjusted to best remove the oscillations. As

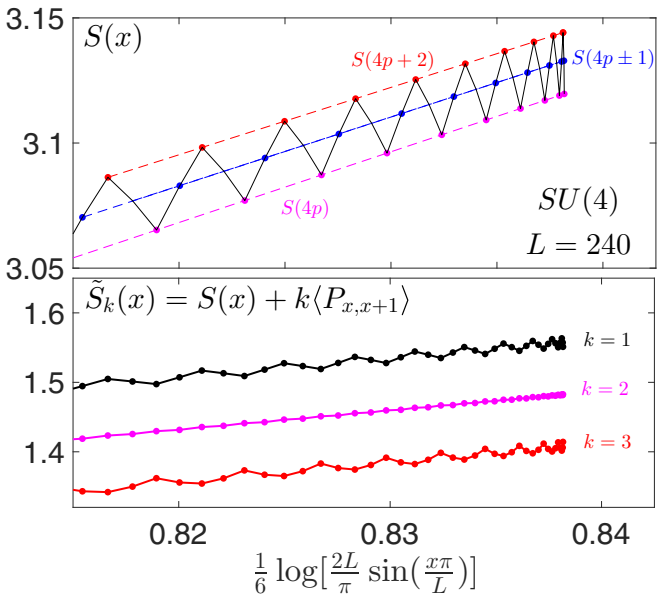

FIG. 9. Top: Entanglement entropy $S(x)$ as a function of the logarithm of the conformal distance $\frac{1}{6}\log[\frac{2L}{\pi}\sin(\frac{\pi x}{L})]$ for an open chain of $L=240$ and SU(4). The position x can be written as $x=4\times p+q$ (with $q=0,1,2,3$), giving rise to three different straight lines: in magenta for $q=0$, in blue for $q=1,3$ or $q=\pm1$, and in red for $q=2$. The corresponding slopes are c_q, and here we have $c_0\approx 2.83$, $c_{1,3}=c_{\pm1}\approx 2.76$, and $c_2\approx 2.70$. Bottom: to remove Friedel oscillations, one can alternatively consider $\tilde{S}_k(x)=S(x)+k\langle P_{x,x+1}\rangle$ (see text for details). Here, the parameter $k=2$ allows one to subtract the oscillations and lead to a straight line of slope $\tilde{c}\approx 2.75$. It is a general observation that $c_{N/2}\leqslant\tilde{c}\leqslant c_0$.

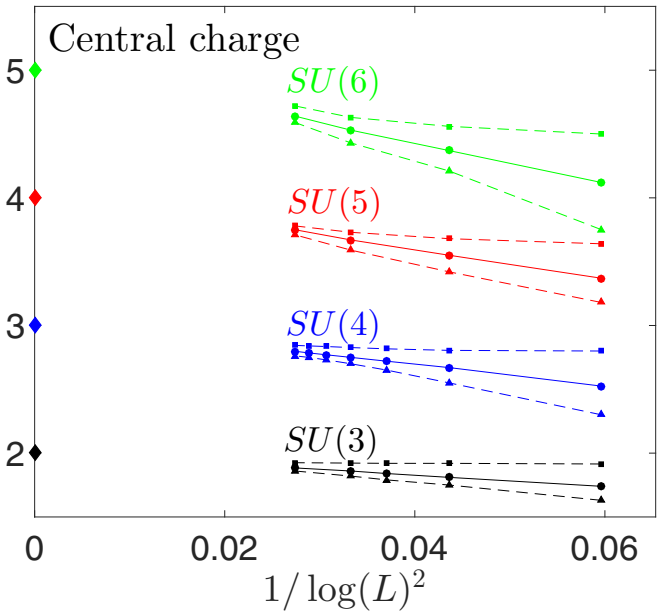

FIG. 10. Fitted central charges for SU(3) up to SU(6) from $L=60$ to $L=420$, as a function of $1/\log(L)^2$: $\tilde{c}$ (solid circles), c_0 (squares), and $c_{N/2}$ (triangles). These estimates of the central charges, all based on the DMRG calculation of the entanglement entropy, are defined in the main text. Diamonds correspond to the theoretical $SU(N)_1$ central charges, $c_{\text{th}}=N-1$. The finite-size central charges are consistent with the theoretical values in the thermodynamic limit.

shown in the bottom panel of Fig. 9, it appears that for SU(4), one should take $k=2$. The best value of k is N dependent but does not change with L. The best parameters k were thus found to be $k=1,2,3.5$, and 6 for $N=3,4,5$, and 6, respectively. For theses values of k, we then fit $\tilde{S}_k(x)$ as a function of the logarithmic of the conformal distance to obtain $\tilde{c}$. We have systematically observed that $c_{N/2}\leqslant\tilde{c}\leqslant c_0$.

To discuss the finite-size effects, we note that for SU(2) the corrections to the central charge are logarithmic with an exponent that depends on the boundary conditions. The correction is positive and scales as $1/\log(L)^3$ for PBC [44,45], while it is negative and scales as $1/\log(L)^2$ for OBC [46,47]. By analogy, we have plotted in Fig. 10 the quantities $c_{N/2}$, $\tilde{c}$, and c_0 as a function of $1/\log(L)^2$ for different values of N. The finite-size effects are negative, as expected for open boundary conditions, and large, but the results are consistent with the theoretical values $c_{\text{th}}=N-1$ expected for $SU(N)_1$ in the thermodynamic limit. For instance, for SU(5), $\tilde{c}\approx 3.37$ for $L=60$, while for $L=420$, we have $\tilde{c}\approx 3.75$, much closer to the thermodynamical limit $c_{\text{th}}=4$. Note that the finite-size effects are much stronger than with PBC, as revealed by a comparison with the DMRG results of Ref. [48] for SU(3) and SU(4). This is consistent with the SU(2) result quoted above that the finite-size corrections to the central charge are in $1/\log(L)^3$ for PBC and in $1/\log(L)^2$ for OBC. Work is in progress to extend our algorithm to PBC and to extend the conformal field analysis to SU(N) with $N>2$ to derive the precise form of the finite-size scaling for general N.

V. CONCLUSIONS AND PERSPECTIVES

To conclude, we have presented an efficient DMRG algorithm to study the SU(N) Heisenberg model that takes into account the full SU(N) symmetry. The efficiency of this algorithm relies on a systematic use of the orthogonal representation of the symmetric group to shortcut the calculation of many SU(N) group theory coefficients needed in the computation. In particular, we have shown how to calculate the matrix elements of the interblock interaction term from the permutational subduction coefficients. The calculation of these coefficients is essentially based on Chen's method, with an improvement that makes the calculation for larger N much lighter. We have applied our method to calculate the ground-state energies and the entanglement entropies of the Heisenberg SU(N) chains with one particle per site and with OBC for several hundreds of sites. Our results agree well with both the exact SU(N) ground-state energies obtained from the Bethe ansatz (in Sec. III) and with the central charges associated to the expected $SU(N)_1$ CFT. They also point to significant finite-size effects when calculating the central charge. The magnitude of these finite-size effects increases with N for a given length of the chain, calling for a better and more systematic understanding of the finite-size effects in the future.

From a methodological point of view, we plan to make several developments that are related to relevant open physical questions. First of all, we would like to implement the calculation of the subduction coefficients when the outer multiplicity

is strictly larger than 1. This will enable us to build the matrix representing the Hamiltonian of the entire chain on a target irrep that does not necessarily contain the ground state, and thus to access some excited states of the full Hilbert space which are states of minimal energy in their sector.

Second, we would like to generalize the procedure to situations where the irrep on each site is not the fundamental one anymore. For instance, we would like to study the case where the irrep on each site is the fully symmetric one in order to check the generalization of the Haldane conjecture to SU(N). Numerically, this problem has already been studied for $N = 3,4$ [49], but many questions remain open [including for SU(3) and SU(4)] [17]. Following the recent analytical filed theory approach [50], the SU(3) Heisenberg chain with the fully symmetric irrep $\square\square\square$ on each site should be gapped. A natural question to be addressed by DMRG is the value of this gap in the thermodynamical limit. Moreover, since our DMRG algorithm keeps track of the SU(N) irrep of each state, we could take advantage of it to characterize the nontrivial edge state structure appearing in the case of OBC. One could also study the case of antisymmetric irreps on each site. For instance, the SU(6) Heisenberg chain with two particles per site in the irrep [1,1] is believed to be gapped [51,52], but the calculation of this gap still needs to be done. In addition, with mixed irreps at each site, one could also investigate more sophisticated models such as the SU(N) version of the Affleck-Kennedy-Lieb-Tasaki (AKLT) models [18,53–55]. They involve irreps with multiple rows and multiple columns at each site and can lead to N distinct topological phases [56,57], classified using group cohomology [58,59].

Finally, Young's rules could also be used to implement SU(N) symmetries in tensor networks to study two-dimensional SU(N) Heisenberg models, which could potentially host exotic physical phases [60–67]. Work is currently in progress along these lines.

ACKNOWLEDGMENTS

We acknowledge useful discussions with Jean-Sébastien Caux, Natalia Chepiga, Luc Frappat, Samuel Gozel, and Wen-Li Yang. This work was supported by the Swiss National Science Foundation. The calculations were performed using the facilities of the Scientific IT and Application Support Center of EPFL.

APPENDIX

1. Irreps of SU(N)

In general, for a system of n particles, each irrep of SU(N) can be associated with a Young diagram composed of n boxes arranged in at most N rows. This represents a particular set of SU(N)-symmetric n-particle wave functions. The shape α of the Young diagram is specified by a partition $\alpha = [\alpha_1,\alpha_2,\ldots,\alpha_k]$ (with $1 \leqslant k \leqslant N$ and $\sum_{j=1}^{k} \alpha_j = n$), where the row lengths α_j satisfy $\alpha_1 \geqslant \alpha_2 \geqslant \cdots \geqslant \alpha_k \geqslant 1$. The diagram can be filled with numbers from 1 to n, and the resulting tableau is said to be *standard* if the entries are increasing from left to right in every row and from top to bottom in every column. Standard Young tableaux (SYTs) play a central role in the representation theory of the symmetric group.

Using $[1] = \square$ to denote the fundamental irrep, the set of all n-particle wave functions lives in the full Hilbert space $\square^{\otimes n}$. The multiplicity f^α of irrep α in this space is equal to number of SYTs with shape α. This number can be calculated from the hook length formula,

$$f^\alpha = \frac{n!}{\prod_{i=1}^{n} l_i}, \tag{A1}$$

where the hook length l_i of the ith box is defined as the number of boxes to the right of it in the same row, plus the number of boxes below it in the same column, plus one (for the box itself). The dimension d_N^α of the irrep can also be calculated from the shape as

$$d_N^\alpha = \prod_{i=1}^{n} \frac{N+\gamma_i}{l_i}, \tag{A2}$$

where γ_i is the algebraic distance from the ith box to the main diagonal, counted positively (resp. negatively) for each box above (resp. below) the diagonal. The full Hilbert space can be decomposed as

$$\square^{\otimes n} = \oplus_\alpha V^\alpha, \tag{A3}$$

where V^α is the sector corresponding to irrep α (and if $d_N^\alpha > 1$, V^α can itself be decomposed into d_N^α equivalent subsectors, $V^\alpha = \oplus_{i=1}^{d_N^\alpha} V_i^\alpha$). The equation for the dimension of the full Hilbert space thus reads

$$N^n = \sum_\alpha f^\alpha d_N^\alpha, \tag{A4}$$

where the sum runs over all Young diagrams with n boxes and no more than N rows.

As an example, for $n = 2$, $\square^2$ can be decomposed as a sum of the subspace spanned by the symmetric two-particle wave functions and of that spanned by the antisymmetric two-particle wave functions:

$$\square^{\otimes 2} = \square \otimes \square = \square\square \oplus \begin{array}{l}\square\\\square\end{array}.$$

There is only one SYT for each of the diagrams [2] and [1,1], so $f^{[2]} = f^{[1,1]} = 1$, while Eq. (A2) gives $d_N^{[2]} = \frac{N(N+1)}{2}$ and $d_N^{[1,1]} = \frac{N(N-1)}{2}$. It is easy to check that Eq. (A4) is satisfied.

2. Young's orthogonal representation of the symmetric group

This section summarizes some useful results concerning the orthogonal representation of the symmetric group. For a given tableau shape α, a convenient representation of the symmetric group $\mathcal{S}_n$ can be formulated using Young's *orthogonal units* $\{o_{rs}^\alpha\}_{r,s=1\ldots f^\alpha}$. These are specific linear combinations of permutations whose explicit forms are not needed here (but could be explicitly calculated [18,20]). They satisfy orthonormality,

$$o_{rs}^\alpha o_{uv}^\beta = \delta^{\alpha\beta}\delta_{su} o_{rv}^\alpha \quad \forall r,s = 1\ldots f^\alpha, \forall u,v = 1\ldots f^\beta, \tag{A5}$$

as well as completeness,

$$\sum_\alpha \sum_{r=1}^{f^\alpha} o_{rr}^\alpha = Id,$$

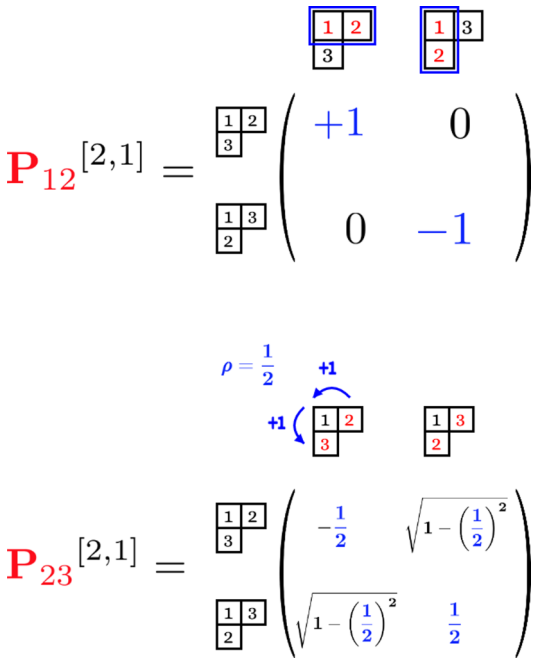

FIG. 11. The matrix representations of permutation operators P_{12} and P_{23} in the basis of SYTs of shape $\alpha = [2,1]$. We have labeled $\begin{smallmatrix}1&2\\3\end{smallmatrix} = S_1$ and $\begin{smallmatrix}1&3\\2\end{smallmatrix} = S_2$. For P_{12}, the numbers 1 and 2 are in the same row on S_1 and in the same column on S_2. For P_{23}, the axial distance between 1 and 2 on S_1 is 2, so $\rho = \frac{1}{2}$. S_2 is the tableau obtained from S_1 by interchanging 1 and 2, and we apply Eq. (A7) accordingly.

and form a basis in which any linear superposition η of permutations belonging to $\mathcal{S}_n$ can be uniquely decomposed as

$$\eta = \sum_{\alpha,r,s} \mu^{\alpha}_{rs}(\eta) o^{\alpha}_{rs}, \tag{A6}$$

where $\mu^{\alpha}_{rs}(\eta)$ are real coefficients.

An important result we will make frequent use of is that successive transpositions $P_{k,k+1}$, i.e., permutations between the consecutive numbers k and $k+1$ ($1 \leqslant k \leqslant n-1$), take an extremely simple form in the basis of orthogonal units. If we write $P_{k,k+1} = \sum_{\alpha,t,q} \mu^{\alpha}_{tq}(P_{k,k+1}) o^{\alpha}_{tq}$, then, for a given shape β, the matrices $\bar{\bar{\mu}}^{\beta}(P_{k,k+1})$ defined by

$$[\bar{\bar{\mu}}^{\beta}(P_{k,k+1})]_{tq} = \mu^{\beta}_{tq}(P_{k,k+1})$$

are symmetric and orthogonal, and very sparse, with at most two nonzero entries in each row and in each column. These entries can be explicitly calculated as follows. We first assign some fixed order (named *last letter order*) to the f^{α} SYTs: Two standard tableaux S_r and S_s are such that $S_r < S_s$ if the number n (which is the last one) appears in S_r in a row below the one in which it appears in S_s. If those rows are the same, one looks at the rows with $n-1$, etc. Thus, we can label the SYTs $S_1, \ldots, S_{f^{\beta}}$. Then, if k and $k+1$ are in the same row (resp. column) in the tableau S_t, we will have $\mu^{\beta}_{tt}(P_{k,k+1}) = +1$ (resp. -1), and all other matrix elements involving t will vanish. If k and $k+1$ are not in the same column nor the same row in S_t, and if S_q is the tableau obtained from S_t by interchanging k and $k+1$, then the only nonvanishing matrix elements involving t or u are given by

$$\begin{pmatrix} \mu^{\beta}_{tt}(P_{k,k+1}) & \mu^{\beta}_{tq}(P_{k,k+1}) \\ \mu^{\beta}_{qt}(P_{k,k+1}) & \mu^{\beta}_{qq}(P_{k,k+1}) \end{pmatrix} = \begin{pmatrix} -\rho & \sqrt{1-\rho^2} \\ \sqrt{1-\rho^2} & \rho \end{pmatrix}. \tag{A7}$$

Here, ρ is the inverse of the *axial distance* from k to $k+1$ on S_t, which is computed by counting $+1$ (resp. -1) for each step made downward or to the left (resp. upward or to the right) to reach $k+1$ from k.

These simple yet incredibly useful formulas (that we call *Young rules*) are clarified in Fig. 11. Moreover, since every permutation can be factorized into successive transpositions, we can use these rules to write the exact matrix representation of any permutation or linear superposition thereof via a few elementary calculations.

3. Calculation of the IRF weights in the SU(2) case using the SYTs and the Young rules

We calculate here the IRF weights for the SU(2) Heisenberg model, which appear in Table 2, p. 520 of [28]. Contrary to what has been done in [28], we do not perform this calculation using the 6j symbols (see Eq. (61) of [28]), but rather using the SYTs and Young's rules, which are much simpler. First, we can establish a connection between the notations appearing in Fig. 6 and in Sec. II B 2 of the present manuscript and those which appear in Table 2, p. 520 of [28]:

$$\begin{aligned} \chi &\leftrightarrow a \\ \beta &\leftrightarrow c \\ \alpha' &\leftrightarrow d \\ \alpha &\leftrightarrow b. \end{aligned} \tag{A8}$$

The coefficient

$$R\begin{pmatrix} & d & \\ a & & c \\ & b & \end{pmatrix} \tag{A9}$$

is equal to the matrix element of P_{N_s,N_s+1} between a state $|\eta\rangle$ and a state $|\xi\rangle$, which both live in the irrep c and which were both built from a common "grandfather" (that one can call $|\Psi\rangle$) by adding twice the fundamental irrep (spin 1/2), corresponding to site N_s and site N_s+1. The common "grandfather" $|\Psi\rangle$ is in the irrep a. For the state $|\eta\rangle$, after adding the first fundamental irrep, the resulting state ("$|\eta^-\rangle$"), who is the direct ascendant (or "father") of $|\eta\rangle$, lives in irrep b, while the father of $|\xi\rangle$ ("$|\xi^-\rangle$") lives in irrep d. One can also use chains of irreps to characterize these two states:

$$|\eta\rangle : |\Psi\rangle \in a \to |\eta^-\rangle \in b \to |\eta\rangle \in c \text{ or } |\eta\rangle : a \to b \to c,$$
$$|\xi\rangle : |\Psi\rangle \in a \to |\xi^-\rangle \in d \to |\xi\rangle \in c \text{ or } |\xi\rangle : a \to d \to c.$$

Now, for SU(2), one can label the irreps either by the value of the total spin j or by using Young diagrams $[\alpha_1,\alpha_2]$,

where $\alpha_1 - \alpha_2 = 2j$. Thus the coefficient

$$R\begin{pmatrix} & j+1/2 & \\ j & & j \\ & j+1/2 & \end{pmatrix} \tag{A10}$$

is equal to

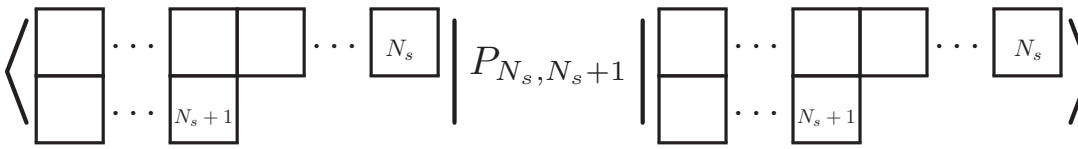

$$= \frac{-1}{2j+1}, \tag{A11}$$

where we have just used the rule described in the previous section about the diagonal term of the matrix representing P_{N_s,N_s+1}, with $2j+1$ the axial distance between N_s and N_s+1 since the young diagram is such that $\alpha_1 - \alpha_2 = 2j$. It also directly follows that

$$R\begin{pmatrix} & j+1/2 & \\ j & & j \\ & j-1/2 & \end{pmatrix} =$$

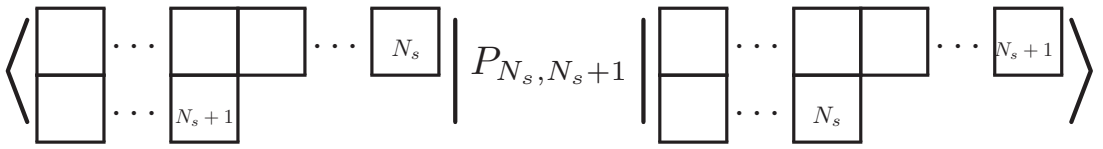

$$= \sqrt{1-(\frac{1}{2j+1})^2} = \frac{\sqrt{2j(2j+2)}}{2j+1}, \tag{A12}$$

using the rule for the off-diagonal term of the matrix representing P_{N_s,N_s+1}, with $2j+1$ the axial distance between N_s and N_s+1. One also finds

$$R\begin{pmatrix} & j & \\ j-1/2 & & j+1/2 \\ & j & \end{pmatrix} =$$

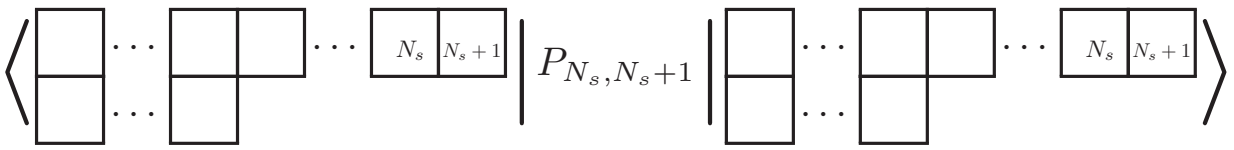

$$= 1. \tag{A13}$$

The other coefficients can be calculated in exactly the same way. We see that the Young's rules allow one to completely bypass the calculation of the $6j-symbols$ to obtain the IRF weights. For spin 1, the IRF weights obtained by Tatsuaki [31] can also be easily calculated using SYTs and the rules we developed for the case of a purely symmetric irrep [17]. Finally, we want to point out that the SU(2) case is very specific: all the coefficients needed for the DMRG can be expressed in terms of IRF weights. In particular, the interblock interaction can be easily written in term of the IRF weights in Nishino and Sierra's approach [28]. The underlying reason is that for SU(2), an irrep is equal to its conjugate. Such a fact manifests itself into some symmetries between the $6j-symbols$.

[1] C. Wu, J.-p. Hu, and S.-c. Zhang, Phys. Rev. Lett. **91**, 186402 (2003).

[2] C. Honerkamp and W. Hofstetter, Phys. Rev. Lett. **92**, 170403 (2004).

[3] M. A. Cazalilla, A. F. Ho, and M. Ueda, New J. Phys. **11**, 103033 (2009).

[4] A. V. Gorshkov, M. Hermele, V. Gurarie, C. Xu, P. S. Julienne, J. Ye, P. Zoller, E. Demler, M. D. Lukin, and A. M. Rey, Nat. Phys. **6**, 289 (2010).

[5] S. Taie, R. Yamazaki, S. Sugawa, and Y. Takahashi, Nat. Phys. **8**, 825 (2012).

[6] G. Pagano, M. Mancini, G. Cappellini, P. Lombardi, F. Schäfer, H. Hu, X.-J. Liu, J. Catani, C. Sias, M. Inguscio, and L. Fallani, Nat. Phys. **10**, 198 (2014).

[7] F. Scazza, C. Hofrichter, M. Höfer, P. C. De Groot, I. Bloch, and S. Fölling, Nat. Phys. **10**, 779 (2014).
[8] X. Zhang, M. Bishof, S. L. Bromley, C. V. Kraus, M. S. Safronova, P. Zoller, A. M. Rey, and J. Ye, Science **345**, 1467 (2014).
[9] C. Hofrichter, L. Riegger, F. Scazza, M. Höfer, D. R. Fernandes, I. Bloch, and S. Fölling, Phys. Rev. X **6**, 021030 (2016).
[10] B. Frischmuth, F. Mila, and M. Troyer, Phys. Rev. Lett. **82**, 835 (1999).
[11] F. F. Assaad, Phys. Rev. B **71**, 075103 (2005).
[12] L. Bonnes, K. R. A. Hazzard, S. R. Manmana, A. M. Rey, and S. Wessel, Phys. Rev. Lett. **109**, 205305 (2012).
[13] L. Messio and F. Mila, Phys. Rev. Lett. **109**, 205306 (2012).
[14] T. C. Lang, Z. Y. Meng, A. Muramatsu, S. Wessel, and F. F. Assaad, Phys. Rev. Lett. **111**, 066401 (2013).
[15] A. Alex, M. Kalus, A. Huckleberry, and J. von Delft, J. Math. Phys. **52**, 023507 (2011).
[16] P. Nataf and F. Mila, Phys. Rev. Lett. **113**, 127204 (2014).
[17] P. Nataf and F. Mila, Phys. Rev. B **93**, 155134 (2016).
[18] K. Wan, P. Nataf, and F. Mila, Phys. Rev. B **96**, 115159 (2017).
[19] A. Young, Proc. London. Math. Soc. **34**, 196 (1931).
[20] D. E. Rutherford, *Substitutional Analysis* (Edinburgh University Press, Edinburgh, UK, 1948).
[21] H. Weyl, *The Theory of Groups and Quantum Mechanics* (Dover Publications, New York, 1931).
[22] S. R. White and D. A. Huse, Phys. Rev. B **48**, 3844 (1993).
[23] S. Daul, Eur. Phys. J. B **14**, 649 (2000).
[24] S. Östlund and S. Rommer, Phys. Rev. Lett. **75**, 3537 (1995).
[25] H. Sakamoto and K. Kubo, J. Phys. Soc. Jpn. **65**, 3732 (1996).
[26] I. P. McCulloch, J. Stat. Mech. (2007) P10014.
[27] I. P. McCulloch and M. Gulácsi, Europhys. Lett. **57**, 852 (2002).
[28] G. Sierra and T. Nishino, Nucl. Phys. B **495**, 505 (1997).
[29] A. Weichselbaum, Ann. Phys. **327**, 2972 (2012).
[30] K. Pilch and A. N. Schellekens, J. Math. Phys. **25**, 3455 (1984).
[31] W. Tatsuaki, Phys. Rev. E **61**, 3199 (2000).
[32] C. Itzykson and M. Nauenberg, Rev. Mod. Phys. **38**, 95 (1966).
[33] J. P.. F. W. Jin-Quan Chen, *Group Representation Theory for Physicists* (World Scientific, Singapore, 2002).
[34] H. Johannesson, Nucl. Phys. B **270**, 235 (1986).
[35] F. C. Alcaraz and M. J. Martins, J. Phys. A: Math. Gen. **22**, L865 (1989).
[36] A. Doikou and R. I. Nepomechie, Nucl. Phys. B **521**, 547 (1998).
[37] D. Arnaudon, N. Crampé, A. Doikou, L. Frappat, and E. Ragoucy, J. Stat. Mech. (2005) P02007.
[38] N. Crampé, L. Frappat, and E. Ragoucy, J. Stat. Mech. (2007) P03014.
[39] F. Wen, T. Yang, Z. Yang, J. Cao, K. Hao, and W.-L. Yang, Nucl. Phys. B **915**, 119 (2017).
[40] B. Sutherland, Phys. Rev. B **12**, 3795 (1975).
[41] S. R. Manmana, K. R. A. Hazzard, G. Chen, A. E. Feiguin, and A. M. Rey, Phys. Rev. A **84**, 043601 (2011).
[42] P. Calabrese and J. Cardy, J. Stat. Mech. (2004) P06002.
[43] S. Capponi, P. Lecheminant, and M. Moliner, Phys. Rev. B **88**, 075132 (2013).
[44] I. Affleck, D. Gepner, H. J. Schulz, and T. Ziman, J. Phys. A: Math. Gen. **22**, 511 (1989).
[45] T. Ziman and H. J. Schulz, Phys. Rev. Lett. **59**, 140 (1987).
[46] C. J. Hamer, G. R. W. Quispel, and M. T. Batchelor, J. Phys. A: Math. Gen. **20**, 5677 (1987).
[47] I. Affleck and S. Qin, J. Phys. A: Math. Gen. **32**, 7815 (1999).
[48] M. Fuhringer, S. Rachel, R. Thomale, M. Greiter, and P. Schmitteckert, Ann. Phys. **17**, 922 (2008).
[49] S. Rachel, R. Thomale, M. Fuhringer, P. Schmitteckert, and M. Greiter, Phys. Rev. B **80**, 180420 (2009).
[50] M. Lajkó, K. Wamer, F. Mila, and I. Affleck, Nucl. Phys. B **924**, 508 (2017).
[51] I. Affleck, Nucl. Phys. B **305**, 582 (1988).
[52] J. Dufour, P. Nataf, and F. Mila, Phys. Rev. B **91**, 174427 (2015).
[53] I. Affleck, T. Kennedy, E. H. Lieb, and H. Tasaki, Phys. Rev. Lett. **59**, 799 (1987).
[54] M. Greiter and S. Rachel, Phys. Rev. B **75**, 184441 (2007).
[55] T. Morimoto, H. Ueda, T. Momoi, and A. Furusaki, Phys. Rev. B **90**, 235111 (2014).
[56] H. Nonne, M. Moliner, S. Capponi, P. Lecheminant, and K. Totsuka, Europhys. Lett. **102**, 37008 (2013).
[57] S. Capponi, P. Lecheminant, and K. Totsuka, Ann. Phys. **367**, 50 (2016).
[58] K. Duivenvoorden and T. Quella, Phys. Rev. B **87**, 125145 (2013).
[59] K. Duivenvoorden and T. Quella, Phys. Rev. B **86**, 235142 (2012).
[60] M. Hermele, V. Gurarie, and A. M. Rey, Phys. Rev. Lett. **103**, 135301 (2009).
[61] M. Hermele and V. Gurarie, Phys. Rev. B **84**, 174441 (2011).
[62] P. Lecheminant and A. M. Tsvelik, Phys. Rev. B **95**, 140406 (2017).
[63] Y. Fuji and P. Lecheminant, Phys. Rev. B **95**, 125130 (2017).
[64] J. Dufour and F. Mila, Phys. Rev. A **94**, 033617 (2016).
[65] P. Nataf, M. Lajkó, A. Wietek, K. Penc, F. Mila, and A. M. Läuchli, Phys. Rev. Lett. **117**, 167202 (2016).
[66] P. Nataf, M. Lajkó, P. Corboz, A. M. Läuchli, K. Penc, and F. Mila, Phys. Rev. B **93**, 201113 (2016).
[67] F. H. Kim, K. Penc, P. Nataf, and F. Mila, Phys. Rev. B **96**, 205142 (2017).